Theoretical investigation of entropy generation and heat transfer by forced convection of copper-water nanofluid in a porous channel - Local thermal non-equilibrium and partial filling effects

Mohsen Torabi [a], Craig Dickson [b], Nader Karimi [1, b]

[a] The George W. Woodruff School of Mechanical Engineering, Georgia Institute of Technology, Atlanta, GA 30332, USA

[b] School of Engineering, University of Glasgow, Glasgow G12 8QQ, United Kingdom

Abstract

Forced convection of copper-water nanofluid through a channel partially filled by a centrally located, porous insert is considered. Constant heat flux boundary conditions are imposed on the channel walls and the nanofluid flow is assumed to be hydrodynamically and thermally fully developed. The investigated system is under the local thermal non-equilibrium and two well-established interface models are employed to specify the thermal boundary conditions at the interface of the porous insert and nanofluid flow. Analytical expressions are derived for the temperature fields, Nusselt number and, total and local entropy generations. A parametric study reveals that variations in nanoparticles volumetric concentration only affect the temperature of the nanofluid flow within the clear region. It also shows that regardless of the choice of the porous-nanofluid interface model, addition of nanoparticles can improve the Nusselt number by up to around 15%. However, the local and total entropy generations are found to be strongly depended upon the employed interface model and increase considerably by increasing the concentration of the nanoparticles. It is shown that at high Biot numbers the effects of the interface model upon the thermal and entropic behaviours of the system diminish. This is argued to be related to the approach of the system towards local thermal equilibrium at larger values of Biot number.

Keywords: Nanofluid; forced convection; entropy generation; local thermal non-equilibrium; porous media.

Nomenclature

a_{sf}	Interfacial area per unit volume of porous media (m^{-1})	*Greek Symbols*	
Bi	Biot number, $\frac{a_{sf} h_{sf} h_0^2}{(1-\varepsilon)k_s}$	γ	Ratio of the wall heat flux to the heat flux at the interface, $q_w/q_{\text{interface}}$
$C_{nf,p}$	Specific heat of the nanofluid, (J $kg^{-1}K^{-1}$)	ε	Porosity of the porous medium
Da	Darcy number, K/h_o^2	θ	Dimensionless temperature
D_h	Hydraulic diameter of the channel ($4h_0$)	μ	Viscosity (kg $m^{-1}s^1$)
h_{sf}	Fluid to solid heat transfer coefficient (W $m^{-2}K^{-1}$)	μ_{eff}	Viscosity of the fluid in porous media (kg $m^{-1}s^1$)
h_0	Height of the channel (m)	μ_{nf}	Viscosity of nanofluid (kg $m^{-1}s^1$)
h_p	Porous substrate thickness (m)	ρ	Density, (kg/m^3)
K	Permeability of the porous medium (m^2)	ξ	Constant parameter used in Eq. (43)
k	Ratio of solid effective thermal conductivity	φ_1	Constant parameter defined by Eq. (54a)

1 Corresponding author.
E-mails: Nader.Karimi@glasgow.ac.uk (N.Karimi), Torabi_mech@yahoo.com(M. Torabi)

	to that of the nanofluid, $(1-\varepsilon)k_s/(\varepsilon k_{nf})$		
k_f	Thermal conductivity of the base fluid (W $m^{-1}K^{-1}$)	φ_2	Constant parameter defined by Eq. (54b)
k_{nf}	Thermal conductivity of the nanofluid (W $m^{-1}K^{-1}$)	φ_3	Constant parameter defined by Eq. (54c)
k_p	Thermal conductivity of the solid particles in nanofluid (W $m^{-1}K^{-1}$)	*Subscripts*	
$k_{nf,eff}$	Effective thermal conductivity of the nanofluid, εk_{nf}	*eff*	Effective property
k_s	Thermal conductivity of the solid material in the porous medium (W $m^{-1}k^{-1}$)	*f*	Base fluid
$k_{s,eff}$	Effective thermal conductivity of the solid matrix, $(1-\varepsilon)k_s$	nf_1	Nanofluid in the open region
Nu	Nusselt number		
q	Heat flux (W m^{-2})	nf_2	Nanofluid in the porous medium
S	Ratio of the porous medium thickness to the channel height, h_p/h_0	*nf*	Nanofluid
T	Temperature (*k*)	*p*	Porous medium
u	Longitudinal velocity (m/*s*)	*s*	Solid (referring to the porous medium)
$\overline{u}$	Average velocity	*w*	Wall
u_r	Characteristic velocity, $-\frac{h_0^2}{\mu_{nf}}\frac{\partial p}{\partial x}$	interface	The interface between the porous medium and the clear region
U	Dimensionless velocity, u/u_r		
$\overline{U}$	Dimensionless average velocity	*Superscripts*	
x	longitudinal coordinate (m)		
y	Transverse coordinate (m)	–	Mean value
Y	Dimensionless *y* coordínate, y/h_0	′,″,	First, second, third, and forth
Z	Constant parameter, $Z = \sqrt{R_\mu/Da}$	‴, ⁗	derivatives with respect to *Y*

1. Introduction

Over the last two decades, research on nanofluids has been most intensive [1]. There are, now, large bodies of literature on natural [2, 3, 4] and forced [5, 6, 7] convection of nanofluids in a wide range of configurations. Recently, physical effects and, in particular, the influences of magnetic and electrical fields on convection of nanofluids have been investigated extensively [8, 9, 10]. Nanofluids can be also used in conjunction with porous media to achieve further improvements in heat transfer [1, 4]. Intuitively, the interaction of the superior thermal conductivity of nanofluids with the improved heat transfer characteristics of porous media is expected to result in higher heat transfer rates. The general notion of improving heat transfer in porous media through substitution of ordinary fluids with nanofluids has been, already, confirmed [1, 11, 12]. Nonetheless, so far, most of the research in this area has been focused on natural and mixed convection [1, 13]. Forced convection of nanofluids in porous media has only recently started to attract attention of the research community [14]. This is such that the necessity of further research on forced convection of nanofluids in porous media has been, particularly, stressed in the most recent version of handbook of porous media [4]. Currently, there are only a limited number of articles in this specific area and almost all of these appeared in the last few years. In the followings, an overview of the existing theoretical and numerical studies on forced convection of nanofluids through porous media is put forward.

One of the pioneering works on the forced convection of nanofluids in porous media was conducted by Ghazvini and Shokouhmand [15]. These authors considered the flow of nanofluid in a row of micro-channels as a porous medium problem. The analyses in this work focused on the influences of particles volume fraction and

Brownian–Reynolds number on the temperature fields and rates of heat transfer [15]. Later, Hatami and Ganji [16] used a similar idea to analyse the transfer of heat in a micro-channel heat sink [16]. Maghrebi et al. modelled the problems of simultaneous momentum, heat and nanoparticles transport by convection and diffusion [17]. Their investigation revealed that the Lewis number inversely correlates with the local Nusselt number in the porous channel [17]. Nevertheless, the volume fraction of nanoparticles was found uncorrelated with the variations in Lewis number [17]. In an interesting fundamental work, Habib Matin and Pop [18], investigated the forced convection of nanofluid in a porous channel combined with a mass transfer phenomenon due to a catalytic reaction on the wall [18]. These authors assumed local thermal equilibrium (LTE) and derived analytical solutions for the temperature and concentration fields and the Nusslet number [18]. The results of Habib Matin and Pop [18] showed that higher volume fraction of nanoparticles leads to the higher rates of heat transfer. Ting et al. [19] considered the local thermal non-equilibrium (LTNE) situation in a porous channel saturated with nanofluids, under isoflux boundary conditions. Attention was paid to the influences of viscous dissipation and analytical solutions were derived for the hydrodynamic and temperature fields [19]. Importantly, Ting et al. [19] showed that ignoring the viscous effects can lead to significant over predictions of the rate of heat transfer. Most recently, Ting et al. conducted a similar analysis on a porous channel with asymmetric thermal boundary conditions [20]. Forced convection of heat in a nanofluid saturated porous medium between two parallel plates was investigated theoretically by Nield and Kuznetsov [7]. They considered the diffusion of nanoparticles and assumed local thermal equilibrium between the nanofluid and solid matrix and developed analytical solutions for Nusselt number [7].

Almost all existing investigations conducted on the problem of nanofluid forced convection in porous conduits have considered fully-filled channels. An exception to this is the numerical work of Servati et al. [21]. In this study the effects of an imposed magnetic field on the forced convection of nanofluid in a partially-filled porous channel, subject to constant wall temperatures, were investigated numerically [21]. Servati et al. showed that, similar to that observed in full porous channels, addition of nanoparticles to partially-filled porous channels could cause considerable increases in the Nusselt number [21]. Further, in a recent work, Siavashi et al. [22] studied forced convection of nanofluid in a pipe containing porous inserts. These authors considered a two-phase model of nanofluid along with fully or partially filled conduits and conducted the first and the second laws analyses of the composite system [22]. They showed that the configurational characteristics of the problem have pronounced impacts on its thermal behaviour and that the partial filling of the pipe strongly affects the heat transfer, pressure drop and entropy generation [22]. This study clearly demonstrated the significance of partially-filled conduits in forced convection of nanofluid in porous media. It is, however, essential to note that Siavashi et al. [22] did not consider the LTNE effects and therefore the applicability of their results is limited to the validity rang of the LTE assumption.

The literature on forced convection of nanofluid in porous media also includes a few studies concerning heat transfer in rotating configurations. In their numerical work, Bachok et al. [23] studied the flow and heat transfer of nanofluids in a configuration involving rotating porous disks. These authors used two different models of the effective thermal conductivity and examined the flow and thermal behaviours of the composite system [23].The flow between counter-rotating disks with porous faces was numerically investigated by Hatami et al. [24]. In their study, mixtures of water with a number of metal and metal oxide nanoparticles were considered. The work of Hatami et al. [24] included an extensive study on the influences of nanoparticle size

and type upon the thermal behaviour of the system. Hosseini et al. [25] employed homotopy perturbation method to analyse the problem of nanofluid flow and heat transfer between rotating porous disks. In keeping with the previous findings for channel flows, these authors [25] showed that in rotating flows increasing the concentration of nanoparticles signifies the Nusselt number. The results of Hosseini et al. [25] indicate that there exists a monotonic and nearly linear relationship between the volumetric fraction of nanoparticles and Nusselt number gain.

In addition to heat transfer analysis, entropy generation minimisation is now considered as a powerful method of optimising various thermal systems [26, 27, 28]. In recent years there has been a growing interest in understanding the entropic behaviour of nanofluids and porous systems [12, 29, 30]. Nonetheless, entropic analysis of composite nanofluid-porous systems has, so far, received limited attention [31] and there are only a few recent studies in this area [30, 32, 33, 34]. Many configurations and conditions still remain to be analysed and a general shortage of research in this area has been declared [31]. Entropy generation in forced convection of nanofluids through porous media has been recently analysed by Ting et al. [33, 34]. These authors considered LTNE condition in porous media embedded in micro-channels [34], which may also include internal heat generation in the solid phase [33]. Since the LTNE model has been used in these two investigations, two energy equations for the fluid and solid phases of the porous material of the system were considered [14]. The analyses of Ting et al [29, 30] revealed that in determining the second law efficiency of the system, the size of nanoparticles and aspect ratio of the channel are of high significance. It is essential to note that these works [7, 19] were exclusively concerned with the fully-filled channels and hence partial-filling effects still remain unexplored.

The preceding review of literature reveals a few major points, which could be summarised as follows.

- The general problem of convection of nanofluids through saturated porous media has been investigated to some depth. Nonetheless, most of these efforts have been focused on natural and mixed convection [1] and forced convection of nanofluid in porous media has, comparatively, received much less attention [4].
- Despite some recent attentions to forced convection in nanofluid flow through porous media, a very limited number of configurations have been, so far, analysed. In particular, convection of nanofluids in partially-filled porous channels is still a highly unexplored problem. Given that the corresponding problem with ordinary fluids has already received a significant attention [35, 36, 37], the lack of nanofluids equivalent studies in this area is clear.
- With the exception of a few very recent works [22, 32, 33, 34] there has been no systematic investigation of entropy generation in forced convection of nanofluids in porous channels. Most importantly, the existing works either ignored local non-equilibrium effects or only considered fully-filled channels. In particular, the problem of entropy generation in forced convection of a nanofluid in a partially-filled porous channel under LTNE has not been analysed in the past.

Given these, the current work aims to make advancements in understanding and modelling of forced convection of nanofluids in porous media under LTNE in partially-filled conduits. An important challenge in LTNE analysis of porous media with porous-fluid or solid interfaces is the selection of the appropriate thermal interface model [38, 39]. While a number of interface models have been developed, some of them are more widely used [40]. Yet, there is no generally preferred porous-fluid or solid interface model and the final choice of the interface model is heavily problem dependent [41]. As a result, a porous system is, often, analysed under

different interface models to detect the similarities and disparities between their predictions [37, 42]. It has been, already, demonstrated that for ordinary fluids the thermal interface model can significantly affect the thermal and entropic behaviour of the porous systems [37, 42, 43]. However, currently there is no study on the influences of porous-nanofluid interface models upon the first and second law performances of conduits partially-filled by porous material. Addressing this issue is the main objective of the present work. A partially-filled porous channel saturated with copper-water nanofluid is considered and analytical solutions are developed for the velocity, temperature fields, Nusselt number and entropy generation. Local thermal non-equilibrium condition is applied to the porous medium [43, 44], and the effects of different porous-nanofluid interface models are examined [37, 45]. In particular, the temperature fields, Nusselt number, validity range of LTE assumption and local and total entropy generations are investigated. It is worth noting that, to the best of the authors' knowledge, there is currently no experimental study on the forced convection of nanoparticles in porous systems. Nonetheless, given that the pore density is usually about 5-40 pore per inch [48] there is, at least, around 0.5 mm of space available for each pore. Considering the size of nanoparticles being about 1-100 nm [46, 47], they are still much smaller than the pore size and hence the addition of nanoparticles to porous thermal systems sounds practical.

2. Analytical analyses

2.1. Governing equations

The investigated configuration is illustrated in Fig. 1. A channel accommodating a porous insert is subject to forced convection, in which the working fluid is water containing copper nanoparticles. The channel is assumed to be two dimensional with a height of h_o, while the porous insert is of height h_p. The walls receive a constant heat flux q_w.

It is recalled that the fluid flow and heat transfer analyses of nanofluid flow systems can be performed through two different modelling approaches. First is the single-phase model, which considers homogenous thermo-physical properties for the nanofluid [18, 19, 20, 29]. The second includes a two-component nonhomogeneous equilibrium model of the nanofluid. Compared to the homogeneous model, the latter is more accurate and computationally expensive and is also often not amenable to analytical approaches. The nonhomogeneous model has been considered recently by a number of scholars [10, 22, 49, 50, 51]. In this work, however, due to the analytical nature of the study, the homogeneous model of nanofluid is used.

The following assumptions are maintained throughout the analysis:

- The porous material is homogeneous and isotopic, with constant properties such as porosity and specific heat.
- LTNE condition applies within the porous region and the problem is under steady state.
- The nanofluid flow is laminar and incompressible.
- The nanofluid is considered to be a homogenous medium.
- Thermally and hydrodynamically fully developed flow exists throughout the channel.
- Viscous heat generation is ignored.
- Radiation is ignored, as the emissivity of the material is negligibly small.
- Gravitational effects are assumed to be negligible.

Using the aforementioned assumptions, the Navier-Stokes equations for the momentum balance of the clear flow can be reduced to [37]

$$-\frac{\partial p}{\partial x}+\mu_{nf}\frac{\partial^2 u_{nf}}{\partial y^2}=0. \tag{1}$$

Assuming Da$\leq 10^{-3}$ the inertia term of the momentum equation becomes negligible [52, 40]. Thus, the Darcy-Brinkman model [53] can be used within the porous region,

$$-\frac{\partial p}{\partial x}+\mu_{eff}\frac{\partial^2 u_p}{\partial y^2}-\frac{\mu_{nf}}{K}u_p=0. \tag{2}$$

Transport of thermal energy in the clear flow region reduces to

$$\rho_{nf}c_{nf,p}u_f\frac{\partial T_{nf1}}{\partial x}=k_{nf}\frac{\partial^2 T_{nf1}}{\partial y^2}. \tag{3}$$

Further, transport of thermal energy for the nanofluid within the porous region can be expressed as

$$\rho_{nf}c_{nf,p}u_p\frac{\partial T_{nf2}}{\partial x}=k_{nf,eff}\frac{\partial^2 T_{nf2}}{\partial y^2}+a_{sf}h_{sf}(T_s-T_{nf2}). \tag{4}$$

The energy equation for the solid phase of the porous region can be written as

$$0=k_{s,eff}\frac{\partial^2 T_s}{\partial y^2}-a_{sf}h_{sf}(T_s-T_{nf2}). \tag{5}$$

2.2. Boundary conditions

The following boundary conditions apply to the momentum equations

$$u_{nf}=0, \qquad at\ y=h_0, \tag{6}$$

$$u_{nf}=u_p,\quad \mu_{nf}\frac{\partial u_{nf}}{\partial y}=\mu_{eff}\frac{\partial u_p}{\partial y}, \qquad at\ y=h_{p,} \tag{7}$$

$$\frac{\partial u_p}{\partial y}=0 \qquad at\ y=0\,. \tag{8}$$

The following conditions apply to the energy equations

$$k_{nf}\frac{\partial T_{nf1}}{\partial y}=q_w, \qquad at\ y=h_0, \tag{9}$$

$$T_{nf1}=T_{nf2}, \qquad at\ y=h_p, \tag{10}$$

$$\frac{\partial T_{nf2}}{\partial y}=\frac{\partial T_s}{\partial y}=0, \qquad at\ y=0. \tag{11}$$

Two interface models (Model A and B of Yang and Vafai [38], or model 1A and model 2A of Alazmi and Vafai [39]) are used to describe the distribution of heat at the interface of the porous insert and the clear channel. Here, these two classical models are extended to nanofluid-porous systems by considering the nanofluid as a homogenous phase distinctive from the porous solid phase. Under Model A, it is assumed that the total heat flux is the sum of the conductive fluxes of the nanofluid and porous solid at the interface [37].

$$q_{interface}=k_{nf,eff}\frac{\partial T_{nf}}{\partial y}\Big|_{interface}+k_{s,eff}\frac{\partial T_s}{\partial y}\Big|_{interface}, \tag{12a}$$

$$T_{nf}\big|_{interface}=T_s|_{interface}=T|_{interface}. \tag{12b}$$

For Model B, the heat flux at the interface is distributed equally to the nanofluid and porous solid phases [37, 52, 38].

$$q_{interface}=k_{nf,eff}\frac{\partial T_{nf}}{\partial y}\Big|_{interface}=k_{s,eff}\frac{\partial T_s}{\partial y}\Big|_{interface}. \tag{13}$$

In Eqs. (12) and (13), $T_{interface}$ and $q_{interface}$ refer to the temperature and heat flux respectively; both evaluated at the interface of the porous and clear regions. The average flow velocity by definition is

$$\bar{u} = \frac{1}{h_0}\left[\int_0^{h_p} u_p dy + \int_{h_p}^{h_0} u_{nf} dy\right]. \tag{14}$$

Integrating Eq. (3) from h_p to h_0 and remembering that in the fully developed region $\frac{\partial T_{nf1}}{\partial x} = \frac{\partial T_{nf2}}{\partial x} = \frac{\partial T_{nf}}{\partial x} =$ const, renders

$$\rho_{nf} c_{nf,p} \frac{\partial T_{nf}}{\partial x} \int_{h_p}^{h_0} u_{nf} dy = \left(q_w - q_{interface}\right). \tag{15}$$

Taking the product of Eqs. (4) and (5), integrating from 0 to h_0 and applying Model A yields

$$\rho_{nf} c_{nf,p} \frac{\partial T_{nf}}{\partial x} \int_0^{h_p} u_p dy = q_{interface}. \tag{16}$$

Combining Eq. (15) with Eq. (16) and using Eq. (14) results in

$$\rho_{nf} c_{nf,p} \frac{\partial T_{nf}}{\partial x}\Big|_{Model\ A} = \frac{q_w}{h_0\, \bar{u}}. \tag{17}$$

Model A heat flux can be found by combining Eq. (17) into Eq. (16)

$$\frac{q_{interface}}{q_w}\Big|_{Model\ A} = \frac{1}{h_0\, \bar{u}} \int_0^{h_p} u_p dy. \tag{18}$$

Heat flux according to Model B is found using the same procedure. By combining Eq. (4) with Eq. (5) and integrating across the porous insert and applying the boundary conditions given in Eq. (13), the following equation can be derived

$$\rho_{nf} c_{nf,p} \frac{\partial T_{nf}}{\partial x} \int_0^{h_p} u_p dy = 2\, q_{interface}. \tag{19}$$

Taking Eq. (15), adding it to Eq. (19) and substituting into Eq. (14) renders

$$\rho_{nf} c_{nf,p} \frac{\partial T_{nf}}{\partial x}\Big|_{Model\ B} = \frac{1}{h_0\, \bar{u}}\left(q_w + q_{interface}\right). \tag{20}$$

Model B heat flux can be found by combining Eqs. (19) and (20)

$$\frac{q_{interface}}{q_w}\Big|_{Model\ B} = \frac{\int_0^{h_p} u_p dy}{2\, h_0\, \bar{u} - \int_0^{h_p} u_p dy}. \tag{21}$$

2.3. Normalisations and velocity profiles

The following dimensionless variables are introduced to normalise the equations.

$$\theta|_{Model\ A} = \frac{k_{s,eff}(T - T_{interface})}{q_w h_0}, \tag{22a}$$

$$\theta|_{Model\ B} = \frac{k_{s,eff}(T - T_{s,interface})}{q_w h_0}, \tag{22b}$$

$$\gamma = \frac{q_{interface}}{q_w}, \tag{22c}$$

$$k = \frac{k_{s,eff}}{k_{nf,eff}}, \tag{22d}$$

$$Bi = \frac{h_{sf} a_{sf} {h_0}^2}{k_{s,eff}}, \tag{22e}$$

$$Y = \frac{y}{h_0}, \tag{22f}$$

$$S = \frac{h_p}{h_0}, \tag{22g}$$

$$U = \frac{u}{u_r}, \tag{22h}$$

$$R_k = \frac{k_{nf}}{k_f} = 1 + \frac{3\phi\left(\frac{k_p}{k_f}-1\right)}{\left(\frac{k_p}{k_f}+2\right)-\phi\left(\frac{k_p}{k_f}-1\right)}, \tag{22i}$$

$$R_\mu = \frac{\mu_{nf}}{\mu_f} = \frac{1}{(1-\phi)^{2.5}}, \tag{22j}$$

where k is the effective thermal conductivity of the solid over the nanofluid. The characteristic velocity, u_r, is given by $u_r = -\frac{{h_0}^2}{\mu}\frac{\partial p}{\partial x}$. Equations (22i) and (22j) relate thermal conductivity and viscosity of the base fluid to that of the nanofluid. These models are representative of copper-water nanofluids and were developed by Maxwell-Garnetts and Brinkman, respectively [54, 55], and are discussed in detail by Torabi et al. [29]. The values of $k_p = 401\, W.m^{-1}.K^{-1}$ and $k_f = 0.613\, W.m^{-1}.K^{-1}$ have been considered for thermal conductivity of copper particles and water, respectively. By employing Eqs. (22i) and (22j) and considering three different concentrations for nanoparticles, such as $\phi = 0\%, 2.5\%$ and 5%, the obtained values for R_k and R_μ are tabulated in Table 1. It is noted that although other formulations have been proposed for the effective thermal conductivity and viscosity of nanofluids [56], Maxwell-Garnett effective thermal conductivity equation and Brinkman effective viscosity equations have been used repeatedly in the literature, see for example [8, 57, 58, 59]. In keeping with these recent investigations, these two models have been used in the current work. It is also essential to emphasise that due to the non-dimensionalisation introduced in Eqs. (22), the expressions developed in the rest of this work are somehow independent of the specific choice of thermo-physical models. That is with no change in the rest of the proceeding solutions, the right hand side of Eqs. (22i) and (22j) can be replaced by any other temperature-independent model.

The following normalised relations for the velocity fields can be obtained using the dimensionless parameters.

$$0 = 1 + R_\mu \frac{\partial^2 U_{nf}}{\partial y^2}, \qquad S < Y < 1, \tag{23a}$$

$$0 = 1 + \frac{\partial^2 U_p}{\partial y^2} - \frac{R_\mu}{Da} U_p, \qquad Y < S. \tag{23b}$$

The following boundary conditions apply

$$U_{nf} = 0, \qquad at\ Y = 1, \tag{23c}$$

$$U_{nf} = U_p, \quad R_\mu \frac{\partial U_{nf}}{\partial Y} = \frac{\partial U_p}{\partial Y}, \qquad at\ Y = S, \tag{23d}$$

$$\frac{\partial U_p}{\partial Y} = 0 \qquad at\ Y = 0. \tag{23e}$$

Velocity in the clear region is expressed as

$$U_{nf}(Y) = \left(-\frac{1}{2}Y^2 + AY + B\right)\frac{1}{R_\mu}, \tag{24}$$

where

$$A = S + \frac{Z\,sinh(ZS)(S - 0.5(1 + S^2) + Da)}{Z(S-1)sinh(ZS) - R_\mu cosh(ZS)}, \tag{25a}$$

$$B = \frac{1}{2} - A. \tag{25b}$$

Velocity within the porous insert can be written as

$$U_p(Y) = C\,cosh(ZS) + \frac{Da}{R_\mu}, \tag{26}$$

$$C = \frac{1}{Z\,sinh(Z\,S)}\,(A - S). \tag{27}$$

Applying the non-dimensional parameters listed in Eq. (22) to Eqs. (24) and (26), the dimensionless average velocity can be derived. Starting from Eq. (14) this becomes

$$\bar{U} = S\frac{Da}{R_\mu} + \frac{C}{Z}sinh(ZS) + \frac{1}{R_\mu}\left[-\frac{1}{6}(1 - S^3) + \frac{1}{2}A(1 - S^2) + B(1 - S)\right], \tag{28}$$

where $Z = \sqrt{R_\mu/Da}$.

Model A prediction of the interfacial heat flux can be found be making Eq. (18) dimensionless

$$\gamma|_{Model\ A} = \frac{1}{\bar{U}}\int_0^S U_p dY. \tag{29}$$

Adding Eqs. (26) and (28) renders

$$\gamma|_{Model\ A} = \frac{\frac{C}{Z}sinh(ZS) + \frac{Da}{R_\mu}S}{\frac{Da}{R_\mu}S + \frac{C}{Z}\,sinh(ZS) + \frac{1}{R_\mu}\left[-\frac{1}{6}(1 - S^3) + \frac{1}{2}A(1 - S^2) + B(1 - S)\right]}. \tag{30}$$

The dimensionless form of Eq. (21) can be used to derive a non-dimensional equation expressing the heat flux at the interface according to Model B:

$$\gamma|_{Model\ B} = \frac{\int_0^S U_p dY}{2\,\bar{U} - \int_0^S U_p dY}. \tag{31}$$

By combining Eqs. (26) and (28), Eq. (31) can be written as follows

$$\gamma|_{Model\ B} = \frac{\frac{C}{Z}sinh(ZS) + \frac{Da}{R_\mu}S}{2\left(\frac{Da}{R_\mu}S + \frac{C}{Z}sinh(ZS) + \frac{1}{R_\mu}\left[-\frac{1}{6}(1-S^3) + \frac{1}{2}A(1-S^2) + B(1-S)\right]\right) - \frac{C}{Z}sinh(ZS) + \frac{Da}{R_\mu}S}. \tag{32}$$

2.4 Solid and fluid temperature fields

2.4.1. Model A prediction of the temperature fields

By implementing the non-dimensional parameters discussed in Eq. (22), in particular Eq. (22a) corresponding to Model A, Eqs. (3), (4) and (5) can be used to produce non-dimensional energy balances for the channel. The clear region transport of energy is written as

$$\varepsilon k\frac{U_{nf}}{\bar{U}} = R_k\theta''_{nf1}(Y). \tag{33}$$

The energy equation applied to the nanofluid in the porous insert becomes

$$\frac{U_p}{\bar{U}} = \frac{R_k}{k}\theta''_{nf2}(Y) + Bi\big(\theta_s(Y) - \theta_{nf2}(Y)\big). \tag{34}$$

Finally, in the solid phase

$$0 = \theta_s''(Y) - Bi\left(\theta_s(Y) - \theta_{nf2}(Y)\right). \tag{35}$$

The normalised boundary conditions are expressed as follows

$$R_k\theta_{nf1}'(1) = \varepsilon k, \tag{36}$$

$$\theta_s(S) = \theta_{nf1}(S) = \theta_{nf2}(S) = 0, \tag{37a}$$

$$\theta_s'(0) = \theta_{nf2}'(0) = 0. \tag{37b}$$

The coupled differential Eqs. (34) and (35) can be made into two fourth order ordinary differential equations by differentiating them twice with respect to Y

$$\theta_{nf2}''''(Y) - Bi\left(1 + \frac{k}{R_k}\right)\theta_{nf2}''(Y) = \frac{k}{R_k\bar{U}}\left[-BiU_p(Y) + U_p''(Y)\right], \tag{38}$$

$$\theta_s''''(Y) - Bi\left(1 + \frac{k}{R_k}\right)\theta_s''(Y) = -\frac{k}{R_k\bar{U}}\left[-BiU_p(Y)\right]. \tag{39}$$

Evaluating the second and third derivatives of θ_{nf2} and θ_s at *Y*=S and *Y=0* by substituting Eqs. (37a) and (37b) into Eqs. (34) and (35) renders

$$\begin{aligned} R_k\theta_{nf2}''(S) &= k\frac{U_p(S)}{\bar{U}} & \theta_s''(S) &= 0 \\ \theta_{nf2}'''(0) &= 0 & \theta_s'''(0) &= 0 \end{aligned} \tag{40}$$

By integrating Eq. (33) a prediction for the clear region temperature can be deduced in accordance with Model A. This reads

$$\begin{aligned} \theta_{nf1}(Y)\big|_{Model\ A} = \frac{\varepsilon k}{\bar{U}R_\mu R_k}\Bigg\{&\left(-\frac{Y^4}{24} + A\frac{Y^3}{6} + B\frac{Y^2}{2}\right) + \left(\frac{1}{6} - \frac{A}{2} - B\right)Y - \left(-\frac{S^4}{24} + A\frac{S^3}{6} + B\frac{S^2}{2}\right) \\ &+ S\left(-\frac{1}{6} + \frac{A}{2} + B\right) + \bar{U}R_\mu(Y - S)\Bigg\}. \end{aligned} \tag{41}$$

Eqs. (38) and (39) can be solved to determine the temperature fields within the porous insert. The temperature fields, according to Model A, are given by the following equations for the nanofluid phase and solid phase respectively

$$\begin{aligned} \theta_{nf2}(Y)\big|_{Model\ A} = \frac{k}{\bar{U}R_\mu}\Bigg\{&\frac{C(Z^2 - Bi)[cosh(ZY) - \cosh(ZS)(1 + Z^2\xi)]}{Z^2(Z^2 - \Gamma^2)} \\ &+ \left(\frac{\frac{Bi}{R_k}(Da)}{\Gamma^2}\right)\left(-\xi + \frac{Y^2}{2} - \frac{S^2}{2}\right) + U_p(S)\xi\Bigg\}, \end{aligned} \tag{42}$$

$$\theta_s(Y)\big|_{Model\ A} = -Bi\frac{k}{\bar{U}R_\mu}\left\{\frac{C[cosh(ZY) - \cosh(ZS)(1 + Z^2\xi)]}{Z^2(Z^2 - \Gamma^2)} - \frac{Da}{\Gamma^2R_\mu}\left(-\xi + \frac{Y^2}{2} - \frac{S^2}{2}\right)\right\}. \tag{43}$$

Where $\Gamma = \sqrt{Bi(1+k)}$ and $\xi = \left(\frac{cosh(\Gamma Y)}{\cosh(\Gamma S)} - 1\right)/\Gamma^2$.

2.4.2. Model B prediction of the temperature fields

The energy Eqs. (3), (4) and (5) are made dimensionless by using the same procedures in section 2.4.1 and implementing the Model B boundary condition given in Eq. (22b). In the clear region, the fluid energy equation is expressed as

$$\frac{U_{nf}}{\bar{U}}(1+\gamma) = \frac{R_k}{\varepsilon\, k}\theta''_{nf1}(Y). \tag{44}$$

1 The fluid energy equation in the porous region can be reduced to

$$\frac{U_p}{\bar{U}}(1+\gamma) = \frac{R_k}{k}\theta''_{nf2}(Y) + Bi\big(\theta_s(Y) - \theta_{nf2}(Y)\big). \tag{45}$$

2 Finally, an expression for the solid phase energy can be written as

$$0 = \theta''_s(Y) - Bi\left(\theta_s(Y) - \theta_{nf2}(Y)\right). \tag{46}$$

3 The following boundary equations apply to Model B

$$R_k\theta'_{nf1}(1) = \varepsilon\, k, \tag{47a}$$

$$\theta_{nf1}(S) = \theta_{nf2}(S), \tag{47b}$$

$$\theta'_{nf2}(0) = \theta'_S(0) = 0, \tag{47c}$$

$$R_k\theta'_{nf2}(S) = \gamma\, k, \tag{47d}$$

$$\theta'_s(S) = \gamma, \tag{47e}$$

$$\theta''_s(S) + Bi\,\theta_{nf2}(S) = 0, \tag{47f}$$

$$\theta_s(S) = 0. \tag{47g}$$

4 The following equations are derived by taking the second derivative of Eqs. (45) and (46) with respect to *Y*.

$$\theta''''_{nf2}(Y) - Bi\left(1 + \frac{k}{R_k}\right)\theta''_{nf2}(Y) = \frac{k}{R_k\bar{U}}(1+\gamma)\big[-BiU_p(Y) + U''_p(Y)\big], \tag{48}$$

$$\theta''''_s(Y) - Bi\left(1 + \frac{k}{R_k}\right)\theta''_s(Y) = -Bi\frac{k}{R_k\bar{U}}(1+\gamma)U_p(Y). \tag{49}$$

5 The second and third derivatives of θ_{nf2} and θ_s at *Y=0* can be evaluated using Eq. (47)

$$\theta''''_{nf2}(Y) = R_k\, k\frac{U'_p(0)}{\bar{U}} = 0, \tag{50a}$$

$$\theta'''_s(0) = 0. \tag{50b}$$

By solving Eq. (44), Model B prediction for the temperature in the clear region becomes

$$\theta_{nf1}(Y)\big|_{Model\ B} = \frac{\varepsilon k}{\bar{U}R_\mu R_k}\left[(1+\gamma)\left(-\frac{Y^4}{24} + A\frac{Y^3}{6} + B\frac{Y^2}{2}\right)\right] + O_1Y + O_2, \tag{51a}$$

6

$$O_1 = \frac{\varepsilon k}{\bar{U}R_\mu R_k}\left[(1+\gamma)\left(-\frac{1}{6} + \frac{A}{2} + B\right)\right] + \frac{\epsilon\, k}{R_k}, \tag{51b}$$

7

$$O_2 = \theta_{nf2}(S) - \frac{\varepsilon k}{\bar{U}R_\mu R_k}\left[(1+\gamma)\left(-\frac{S^4}{24} + A\frac{S^3}{6} + B\frac{S^2}{2}\right)\right] - O_1S. \tag{51c}$$

8 Solving Eqs. (48) and (49), and applying boundary conditions (47) and (50) reveals the temperature
9 distributions in the porous region.

$$\theta_{nf2}(Y)\big|_{Model\ B} = \frac{\varphi_1}{\Gamma^2}\cosh(\Gamma Y) + \left[\frac{\frac{kR_\mu}{\bar{U}R_k}(1+\gamma)Bi\,Da}{\Gamma^2}\right]\left(\frac{Y^2}{2}\right) + \frac{k}{\bar{U}R_k}\left(\frac{C(Z^2-Bi)(1+\gamma)}{Z^2(Z^2-\Gamma^2)}\right)\cosh(ZY) + \varphi_3, \tag{52}$$

$$\theta_s(Y)|_{Model\ B} = \frac{\varphi_2}{\Gamma^2}[\cosh(\Gamma Y) - \cosh(\Gamma S)] + \left[\frac{\frac{k}{\overline{U}}\frac{1}{R_k R_\mu}(1+\gamma)Bi\ Da}{\Gamma^2}\right]\left(\frac{Y^2}{2} - \frac{S^2}{2}\right) - \frac{k}{\overline{U}R_k}\left(\frac{C\ Bi(1+\gamma)}{Z^2(Z^2-\Gamma^2)}\right)[\cosh(ZY) - \cosh(ZS)], \tag{53}$$

where

$$\varphi_1 = \frac{\Gamma}{\sinh(\Gamma S)}\left[\frac{k\,\gamma}{R_k} - \frac{\frac{k}{\overline{U}}\frac{R_\mu}{R_k}(1+\gamma)Bi\ Da}{\Gamma^2}S - \frac{k}{\overline{U}R_k}\left(\frac{C(Z^2-Bi)(1+\gamma)}{Z^2(Z^2-\Gamma^2)}\right)\sinh(ZS)\right], \tag{54a}$$

$$\varphi_2 = \frac{\Gamma}{\sinh(\Gamma S)}\left[\gamma - \frac{\frac{k}{\overline{U}}\frac{1}{R_k R_\mu}(1+\gamma)Bi\ Da}{\Gamma^2}S + \frac{Bi\ k}{\overline{U}R_k}\left(\frac{C(1+\gamma)}{Z^2(Z^2-\Gamma^2)}\right)\sinh(ZS)\right], \tag{54b}$$

$$\varphi_3 = \mathrm{Cosh}(\Gamma S)\left[\frac{\varphi_1}{\Gamma^2} - \frac{\varphi_2}{Bi}\right] + \left[\frac{\frac{k}{\overline{U}}\frac{R_\mu}{R_k}(1+\gamma)Bi\ Da}{\Gamma^2}\right]\left(-\frac{1}{Bi} - \frac{S^2}{2}\right) + \frac{Bi\ k}{\overline{U}R_k}\left(\frac{C\ (1+\gamma)}{Z^2(Z^2-\Gamma^2)}\right)\cosh(ZS)\,. \tag{54c}$$

2.4.3 LTE solution

Adding Eqs. (34) and (35) yields

$$\frac{R_k}{k}\theta''_{nf2}(Y) + \theta''_s(Y) = \frac{U_p}{\overline{U}}. \tag{55}$$

.

Application of LTE requiers $\theta_{nf} = \theta_s = \theta$. Therefore, Eq. (55) becomes

$$\left(\frac{R_k}{k} + 1\right)\theta'' = \frac{U_p}{\overline{U}}. \tag{56}$$

The following boundary conditions apply to the one-equation model

$$\frac{\partial\theta}{\partial Y}(y=0) = 0, \qquad \theta(S) = \theta_{nf1}(S). \tag{57}$$

Integrating Eq. (56) and using boundary conditions given in Eq. (57), the LTE temperature field within the porous region of the channel can be written as

$$\theta_p(Y)\big|_{LTE} = \frac{k}{R_k + k}\left\{\frac{1}{\overline{U}}\left(\frac{C[cosh(ZY) - \cosh(ZS)]}{Z^2} + \frac{Da}{R_u}(Y^2 - S^2)\right)\right\}. \tag{58}$$

2.5 Nusselt Number

The Nusselt Number for partial filling can be found using Roshenow and Hartnett [60].

$$Nu = \frac{q_w D_h}{k_f(T_w - T_m)}. \tag{59}$$

Assuming the system is fully developed [41]:

$$Nu = \frac{q_w D_h}{k_{nf,eff}(T_w - T_m)}. \tag{60}$$

The hydraulic diameter is represented here by D_h, which is equal to $4h_0$. By normalising Eqs. (59) and (60) using non-dimensional parameters, the following expressions are obtained.

$$Nu = \frac{4\varepsilon k}{(\theta_w - \theta_m)}. \tag{61}$$

For S=1:

$$Nu = \frac{4\varepsilon}{(\theta_w - \theta_m)}, \tag{62}$$

where,

$$\theta_w = \theta_{nf1}\big|_{Y=1}. \tag{63}$$

θ_m is the non-dimensional mean temperature, and is defined as:

$$\theta_m = \frac{\int_0^S U_p \theta_{nf2} dy + \int_S^1 U_{nf} \theta_{nf1} dy}{\bar{U}}. \tag{64}$$

By solving Eqs. (64) and (63), we can find the Nusselt number according to Eq. (61). This involves very large algebraic equations. Thus, Wolfram Mathematica was used to handle the mathematical manipulations. The resultant relations are quite lengthy and therefore are not shown here.

2.6 Entropy Generation

Equations for local entropy generations can be written as follows [43, 44]:

$$\dot{S}^m\big|_{nf2} = \frac{k_{nf,eff}}{T_{nf2}^2}\left(\left(\frac{dT_{nf2}}{dx}\right)^2 + \left(\frac{dT_{nf2}}{dy}\right)^2\right) + \frac{h_{sf} a_{sf} (T_s - T_{nf2})^2}{T_s T_{nf2}} + \frac{\mu_{nf}}{k T_{nf2}} u_p^2 + \frac{\mu_{nf,eff}}{T_{nf2}}\left(\frac{du_p}{dy}\right)^2 \qquad 0 < y < h_p \tag{65}$$

$$\dot{S}^m\big|_{s} = \frac{k_{s,eff}}{T_s^2}\left(\left(\frac{dT_s}{dx}\right)^2 + \left(\frac{dT_s}{dy}\right)^2\right) + \frac{h_{sf} a_{sf} (T_s - T_{nf2})^2}{T_s T_{nf2}} \qquad 0 < y < h_p \tag{66}$$

$$\dot{S}^m\big|_{nf1} = \frac{k_{nf}}{T_{nf1}^2}\left(\left(\frac{dT_{nf1}}{dx}\right)^2 + \left(\frac{dT_{nf1}}{dy}\right)^2\right) + \frac{\mu_{nf}}{k T_{nf1}} u_{nf}^2 \qquad h_p < y < h_o \tag{67}$$

The dimensionless forms of these equations, in which entropy generation rate is given as $N_s = \frac{\dot{s}^m h_0^2}{k_{s,eff}}$, are shown below:

$$N_s|_{nf2} = \frac{R_k}{k(\theta_{nf2} + B)^2}\left(\left(\frac{(1-\gamma)}{\frac{Pe}{k}\int_S^1 U_{nf} dY}\right)^2 + \left(\frac{d\theta_{nf2}}{dY}\right)^2\right) + \frac{Bi(\theta_s - \theta_{nf2})^2}{(\theta_s + B)(\theta_{nf2} + B)} + \frac{R_\mu Br U_p^2}{Da(\theta_{nf2} + B)} + \frac{R_\mu Br}{\varepsilon(\theta_{nf2} + B)}\left(\frac{dU_p}{dY}\right)^2 \qquad 0 < Y < S \tag{68}$$

$$N_s|_s = \frac{1}{k(\theta_s + B)^2}\left(\left(\frac{(1-\gamma)}{\frac{Pe}{k}\int_S^1 U_{nf} dY}\right)^2 + \left(\frac{d\theta_s}{dY}\right)^2\right) + \frac{Bi(\theta_s - \theta_{nf2})^2}{(\theta_s + B)(\theta_{nf2} + B)} \qquad 0 < Y < S \tag{69}$$

$$N_s|_{nf1} = \frac{R_k}{k\varepsilon(\theta_{nf1}+B)^2}\left(\left(\frac{(1-\gamma)}{\frac{Pe}{k}\int_S^1 U_{nf}dY}\right)^2 + \left(\frac{d\theta_{nf1}}{dY}\right)^2\right) + \frac{BrU_{nf1}^2}{Da(\theta_{nf1}+B)} \qquad S < Y < 1 \qquad (70)$$

where $Pe = \frac{h_0\,\rho_{nf}c_{nf,p}\,\mu}{k_{f,eff}}$, $B = \frac{T_s\,k_{s,eff}}{q_w\,h_0}$ for model A and $B = \frac{T_{s,int}\,k_{s,eff}}{q_w\,h_0}$ for model B.

Finally, we can find the dimensionless total entropy generation rate as follows,

$$N_t = \int_0^1 N_s dY. \qquad (71)$$

3. Results and discussion

This section is divided into three subsections. First, the velocity field, temperature distributions and Nusselt number expressions developed in sections 2 are validated against the previously published results for ordinary fluids. Next, subsection 3.2 provides a comprehensive parametric study on the temperature fields, maximum temperature differences, Nusselt number and heat transfer performance (HTP) of the channel. In this section, influences of the pertinent parameters and the concentration of nanoparticles upon the thermal behaviour of the system are analysed. Finally, subsection 3.3 examines the local and total entropy generation rates within the system under investigation.

3.1. Validation

Figure 2 shows a comparison between the velocity and temperature fields developed in section 2 and those previously reported in the literature for ordinary fluids [37, 40]. Further, the Nusselt number results are compared with the existing expressions for the Nusselt number in the partially-filled channels. In this figure the concentration of nanoparticles has been set to zero and therefore the nanofluid results are reduced to those of the base fluid. The excellent agreement between the current results and those extracted from the literature confirms the validity of the mathematical derivations reported in sections 2.

3.2. Temperature and Nusselt number

Figures 3 and 4 show the temperature distributions of the nanofluid phase across the channel for varying values of the thermal conductivity ratio, Biot number and nanoparticles volumetric concentration. As a general trend, these figures show that the addition of nanoparticles and variation of their concentration have negligible influences on the temperature of the nanofluid phase within the porous region. This remains almost true for all the investigated combinations of the thermal conductivity ratio, Biot number and interface models. In the clear region, however, there is more prominent distinctions between the dimensionless temperatures at different concentrations of the nanoparticles. As a common feature in all temperature plots in Figs. 3 and 4, it is observed that by increasing the nanoparticle concentration the dimensionless temperature of the nanofluid in the clear region decreases. This is in keeping with the physical expectations, as increasing the nanoparticles concentration results in enhancing the thermal conductivity of the nanofluid, which in turn reduces the dimensionless flow temperature.

Assumption of local thermal non-equilibrium in the current work allows for the nanofluid and porous solid to have different local temperatures. For a given dimensionless thickness of the porous insert, the maximum of this temperature difference across the insert, $|\Delta\theta_{max}|$, can be readily calculated. Figure 5 has been constructed

by changing the thickness of the porous thickness from zero to the full channel height and recording $|\Delta\theta_{max}|$ for each thickness. In this figure the concentration of nanoparticles has been varied. Similar to that previously reported for ordinary fluids [37], for small to medium dimensionless insert thickness the maximum temperature difference remains negligible. However, further thickening of the porous insert results in increasing the temperature difference between the solid and nanofluid phases. For values of S>0.8 the maximum temperature difference between nanofluid and solid phases becomes strongly dependent upon the thickness of the porous insert. Figure 5 shows that regardless of the values of Bi and *k* or the type of interface model, the full porous channel always features the highest maximum temperature difference. It is essential to note that addition of nanoparticles has only small influences on this behaviour. For values of S<0.9 there is no meaningful change in the maximum temperature difference when the nanoparticles concentration varies. Nanoparticles can only affect the maximum temperature difference when the channel is nearly fully-filled. It follows that in partially-filled porous channels, the validity of local thermal equilibrium assumption is not influenced by the replacement of ordinary fluid with nanofluid. Hence, the previous findings on the validity of LTE in the partially-filled porous channels, saturated with ordinary fluids, see for example [37], remain applicable to the equivalent nanofluid problems. This result is, of course, limited to the investigated copper-water nanofluid and its validity for other types of nanofluids remains to be verified.

Figures 6 and 7 show the variations of Nusselt number, as defined by Eq. 59, with the changes in the porous insert thickness. Thermal conductivity ratio, Biot number and porous-nanofluid interface models are varied in these two figures, and Nusselt number is plotted against the dimensionless thickness of the porous insert. For the configuration under investigation (Fig. 1), the general behaviour of Nusselt number for ordinary fluids has been already explored [40]. As almost all Nusselt number plots in Figs. 6 and 7 show, there is a strong correlation between the values of Nusselt number and the dimensionless thickness of the porous insert. Nusselt number reaches its maximum value at around S_{opt}~0.8. The optimal value of S and the maximum Nusselt number are determined by the pertinent parameters, which include Bi, *k* and the interface model [40]. Here, the emphasis is on the modifications of Nu due to the addition of nanoparticles. It is clear from Figs. 6 and 7 that nanoparticles have an almost uniform effect on the Nusselt number graphs. At low values of the porous thickness, addition of nanoparticles with high concentration (ϕ=5%) leads to an enhancement of the Nusselt number by around 15%. The exact value of the enhancement appears to be dependent upon the interface model and is slightly higher for Model A. It is also directly related to the concentration of the nanoparticles and by halving the concentration the increase in Nusselt number is also halved. This trend continues up to the maximum value of the Nusselt number. At this point and for ϕ=5%, an enhancement better than 15% for Models A and B for all the investigated combinations of Bi and *k* is evident. Further increasing of the porous insert from the optimal value results in a sharp decrease in the Nusselt number. This behaviour tends to mask the influence of nanoparticles on the enhancement of the Nusselt number. However, a close inspection of Figs. 6 and 7 reveals that the enhancement continues in this region with almost the same strength as for the smaller values of *S*. Figures 7 shows that when Biot number increases from 0.1 in Fig. 7a to 10 in Fig. 7b, the Nusselt number features a minimum value in the vicinity of the fully porous filled condition, i.e. *S*~1. This behaviour, which cannot be seen in Model B, clearly reflects the importance of the interface conditions and their influences on the performance of the system.

It is well known that introduction of nanoparticles is associated with an increase in the viscosity compared to the base fluid. The resultant increase in the friction could potentially contribute to the increase in the pumping

losses. Further, the use of porous insert intensifies the frictional effects while enhances the rate of heat transfer. As a result, nanoparticles and the porous insert have a dual effect. They both signify the rate of heat transfer through enhancing the value of Nusselt number (see Figs. 6 and 7) but they also increase the frictional losses in the flow. The extents of Nusselt number and friction increases are related to the thickness of the porous insert and concentration of the nanoparticles. Hence, a thermo-hydraulic criterion can be introduced to evaluate the combined effects of increasing heat transfer rate and flow friction. Such criterion has been previously devised in the context of heat transfer in porous media and is regarded as heat transfer performance (HTP) [61] and is, now, extended to nanofluids applications. HTP was defined in Ref. [61] as $HTP = \frac{(Nu)_p/(Nu)_0}{(fRe)_p/(fRe)_0}$ where indices 'p' and 'o' refer, respectively, to a channel with and without porous insert. Further, the friction factor, f is defined as [61] $f = \frac{8}{\bar{U}Re}$ where Re is a macroscopic Reynolds number based on the fluid velocity and is given by $Re = \frac{\rho_{nf}\bar{u}h_0}{\mu}$. In Figure 8 the heat transfer performance of the copper-water nanofluid with varying concentration of nanoparticles is investigated at different values of Darcy number of the porous insert. It is clear in this figure that addition of nanoparticles hardly modifies the HTP plots. This is because the increase in the convective heat transfer rate is negated by the slightly greater viscous forces introduced by the addition of nanoparticles. Therefore, although increasing porous thickness significantly reduces the HTP, adding nanoparticles does not. This is an important finding as it implies that adding nanoparticles does not adversely affect the heat transfer performance of the system and that the porous insert remains as the main cause of the pressure drop.

3.3. Local and total entropy generation

Local entropy generation rates for Models A and B, under different values of nanoparticles concentration and Biot number have been illustrated in Figs. 9 and 10. A low value of thermal conductivity ratio has been considered in Fig. 9 and a higher value of *k* was applied to the plots in Fig. 10. It is clear from both of these two figures that the local entropy generation rate increases with an increase in nanoparticles volumetric concentration. This is due to the fact that by increasing the volumetric concentration, the heat transfer through the system increases, which then leads to an increase of entropy generation rates. A significant discontinuity in the local entropy generation rate within the nanofluid phase is observed in Figs. 9 and 10. This discontinuity occurs exactly at the porous-nanofluid interface and is due to the major differences in the thermal characteristics of the porous and clear regions. Such abrupt changes in the local entropy generation have been recently reported in porous systems filled with ordinary fluids [43, 44]. This stresses the fact that the porous-nanofluid interface is a strong source of irreversibility. Further, Figs. 9 and 10 demonstrate that unlike that in the nanofluid phase, the local entropy generation within the solid phase of the porous medium does not strongly dependent on the nanoparticles volumetric concentration. Nonetheless, since the value of local entropy generation within the solid phase is not negligible, this should be included into the calculation of the total entropy generation rate. When Model A is in place, similar to the temperature distribution, Biot number has a negligible impact on the behaviour of entropy generation in the channel. However, under model B Biot number has influential effects on the local entropy generation rate. It is interesting to note that the direction of these influences dependents upon the thermal conductivity ratio and can be either towards increasing or decreasing the rate of entropy generation. Once again, this is similar to the effect of Biot number on the temperature distribution under Model B. This can

be clearly seen in Figs. 9c and 9d. As an important general feature, Figs. 9 and 10 show that regardless of the employed parameters, Model B always predicts a higher rate of local entropy generation.

Figures 11-13 illustrate variations of the total entropy generation rate with Biot number, thermal conductivity ratio, thickness of the porous section and the two considered interface models. For all cases, similar to the local entropy generation rate, the total entropy generation increases with an increase in the nanoparticles volumetric concentration. Similar to that discussed for the temperature distribution and local entropy generation, Biot number does not have a great impact on total entropy generation under Model A. This can be seen clearly in Figure 11a. However, under Model B in Figure 11b, Biot number has a noticeable influence on the total entropy generation rate. For both interface models, increasing Biot number causes a decrease in the total entropy generation rate. Also, in all subfigures, it is observed that once the Biot number exceeds a certain value the total entropy generation remains constant. This can be referred to the fact that increasing Biot number reflects an enhancement of the internal heat exchanges within the porous medium. This, in turn, implies that the problem is approaching the condition of local thermal equilibrium (LTE). Hence, increasing the Biot number does not continue to change the temperature distribution, and therefore local and accordingly total entropy generation rates remain constant. Figure 12 depicts the trend of variations in the total entropy generation versus the thermal conductivity ratio and shows that there is an almost linear relation between the two. Figure 13 illustrates the effects of thickness of the porous insert on the total entropy generation rate. It is observed, in this figure, that this behaviour remains unchanged for the two investigated interface models. Further, this figure shows that, for both models, increasing the thickness of the porous insert from 0 to around 0.6 does not have any significant impact on the value of the total entropy generation rate. However, when the dimensionless porous thickness is increased from 0.6 to 1, which is equal to the height of the channel, the total entropy generation rate sharply increases. Once again, Figs. 12 and 13 demonstrate that inclusion of Model B results in considerably higher entropy generation compared to that calculated under Model A.

The result presented in this section showed the strong dependency of the local and total entropy generation on the concentration of nanoparticles. Further, similar observations can be made about the Nusselt number results (Figs. 6 and 7). A common trend in all entropy generation and Nusselt number figures is their uniform responses to the variations in the nanoparticle concentration. For instance, increasing the nanoparticle concentration leads to a linear increase in the local entropy generation within the clear and porous regions, as shown in in Figs. 8 and 9. Physically, this is due to the increase of thermal conductivity of the nanofluid, which enhances the rate of heat transfer and decreases the fluid temperature (see Figs. 3 and 4) and therefore signifies the generation of entropy. Despite the existence of this qualitative physical picture, the quantitative dependency of entropy generation upon the concentration of nanoparticles is not immediately obvious. Further, Eqs. 22i and 22j show that, in general, there are nonlinear relationships between the concentration of nanoparticles and their conductivity and viscosity ratios. Hence, the almost linear relations between the increase in entropy generation and that of nanoparticle concentration in Figs. 9 and 10 and also Figs. 12 and 13 are striking. It should be noted, however, that the generalisation of this point should be done most cautiously. Different nanofluid thermo-physical models need to be incorporated in the analytical setting of section 2, before reaching a general conclusion about the effects of nanoparticle concentration. This remains as a future task.

4. Conclusions

Thermal and entropic behaviours of a channel containing nanofluid flow and including a central porous insert, were analysed theoretically. In particular, the problems of forced convection of heat and generation of entropy were examined. The condition of LTNE was assumed and analytical expressions were developed for the temperature fields, Nusselt number and local and total entropy generation. The subsequent parametric study revealed the following points.

- Addition of nanoparticles has negligible effects upon the flow temperature inside the porous insert. However, temperature of the flow in the clear region of the channel is affected by the concentration of the nanoparticles.
- Nanoparticles tend to increase the Nusselt number in porous systems. The extent of this variation was found to be directly proportional with the volumetric concentration of the nanoparticles and almost independent of the interface model.
- At 5% volumetric concentration, for the investigated nanofluid, the Nusselt number increases by around 15%. Notably, this fractional increase remains almost the same for all porous insert thicknesses.
- The concept of heat transfer performance, originally developed for forced convection of ordinary fluids within porous media, was extended to nanofluids. It was observed that changes in the concentration of nanoparticles hardly modify HTP and, therefore the large frictions introduced by the porous insert continue to dominate the behaviour of HTP within nanofluid flows.
- The local and total entropy generation of the nanofluid were found to be significantly affected by the variations in the nanoparticles concentrations. This was the case for the flows of nanofluid inside the porous and clear regions. However, the local entropy generation within the solid phase remained almost independent of the concentration of the nanoparticles.
- The local and total entropy generations were found to be strongly dependent upon the choice of the interface model. Between the two investigated interface models, application of Model B was observed to lead to higher irreversibility.

The findings of this paper showed that similar to that encountered in ordinary fluids, interface models can have large effects upon the thermal and entropic behaviours of the porous systems saturated with nanofluids. These effects are, particularly, significant at low Biot numbers, in which the local thermal non-equilibrium effects are strong. Nonetheless, in interpreting the quantitative results of this work, it is important to note the limitations of the nanofluid thermo-physical models used in Eqs. 22i and 22j. It is finally emphasised that the general problem of determining the porous-fluid/solid interface model is still open and the work in this area is ongoing [4]. In the absence of a globally acceptable interface model, it is essential to know the general characteristics of a given thermal system under the commonly used interface models. Provision of such knowledge was the ultimate aim of this study.

References

[1] R. A. Mahdi, H. Mohammed, K. Munisamy and N. Saeid, “Review of convection heat transfer and fluid flow in porous media with nanofluid,” *Renewable and Sustainable Energy Reviews,* vol.

41, pp. 715-734, 2015.

[2] M. Sheikholeslami, M. Ellahi, M. Hassan and S. Soleimani, “A study of natural convection heat transfer in a nanofluid filled enclosure with elliptic inner cylinder.,” *International Journal of Numerical Methods for Heat & Fluid Flow,* vol. 24, no. 8, pp. 1906-1927, 2014.

[3] M. Sheikholeslami and R. Ellahi, “Three dimensional mesoscopic simulation of magnetic field effect on natural convection of nanofluid,” *International Journal of Heat and Mass Transfer,* vol. 89, pp. 799-808.

[4] K. Vafai, Handbook of porous media, third edition, CRC Press, 2015.

[5] M. Sheikholeslami, M. Rashidi and D. Ganji, “Numerical investigation of magnetic nanofluid forced convective heat transfer in existence of variable magnetic field using two phase model,” *Journal of Molecular Liquids,* vol. 212, pp. 117-126, 2015.

[6] M. Sheikholeslami, M. Rashidi and D. Ganji, “Effect of non-uniform magnetic field on forced convection heat transfer of–water nanofluid,” *Computer Methods in Applied Mechanics and Engineering,* vol. 294, pp. 299-312, 2015.

[7] D. Nield and A. Kuznetsov, “Forced convection in a parallel-plate channel occupied by a nanofluid or a porous medium saturated by a nanofluid,” *International Journal of Heat and Mass Transfer,* vol. 70, pp. 430-433, 2014.

[8] M. Sheikholeslami, K. Vajravelu and M. Rashidi, “ Forced convection heat transfer in a semi annulus under the influence of a variable magnetic field,” *International Journal of Heat and Mass Transfer,* vol. 92, pp. 339-348, 2016.

[9] M. Sheikholeslami, M. Rashidi, T. Hayat and D. Ganji, “Free convection of magnetic nanofluid considering MFD viscosity effect,” *Journal of Molecular Liquids,* vol. 218, pp. 393-399, 2016.

[10] M. Sheikholeslami, S. Soleimani and D. Ganji, “Effect of electric field on hydrothermal behavior of nanofluid in a complex geometry,” *Journal of Molecular Liquids,* vol. 213, pp. 153-161, 2016.

[11] O. Pourmehran, M. Rahimi-Gorji, M. Hatami, S. Sahebi and G. Domairry, “Numerical optimization of microchannel heat sink (MCHS) performance cooled by KKL based nanofluids in saturated porous medium,” *Journal of the Taiwan Institute of Chemical Engineers,* 2015.

[12] F. Selimefendigil and H. F. Öztop, “Natural convection and entropy generation of nanofluid filled cavity having different shaped obstacles under the influence of magnetic field and internal heat generation,” *Journal of the Taiwan Institute of Chemical Engineers,* 2015.

[13] B. Hoseinpour, H. Ashorynejad and K. Javaherdeh, “Entropy Generation of Nanofluid in a Porous Cavity by Lattice Boltzmann Method.,” *Journal of Thermophysics and Heat Transfer,* pp. 1-8, 2016.

[14] T. Armaghani, M. Maghrebi, . A. J. Chamkha and M. Nazari, “Effects of Particle Migration on Nanofluid Forced Convection Heat Transfer in a Local Thermal Non-Equilibrium Porous Channel,” *Journal of Nanofluids,* vol. 3, no. 1, pp. 51-59, 2014.

[15] M. Ghazvini and H. Shokouhmand, “Investigation of a nanofluid-cooled microchannel heat sink using fin and porous media approaches,” *Energy conversion and management,* vol. 50, no. 9, pp. 2373-2380, 2009.

[16] M. Hatami and D. Ganji, “Thermal and flow analysis of microchannel heat sink (MCHS) cooled by Cu–water nanofluid using porous media approach and least square method,” *Energy Conversion and management ,* vol. 78, pp. 347-358, 2014.

[17] M. J. Maghrebi, M. Nazari and T. Armaghani, “Forced convection heat transfer of nanofluids in a porous channel,” *Transport in porous media,* vol. 93, no. 3, pp. 401-413, 2012.

[18] M. Habibi Matin and I. Pop, “Forced convection heat and mass transfer flow of a nanofluid through a porous channel with a first order chemical reaction on the wall,” *International Communications in Heat and Mass Transfer,* vol. 46, pp. 134-141, 2013.

[19] T. W. Ting, , Y. M. Hung and N. Guo, “Viscous dissipative forced convection in thermal non-equilibrium nanofluid-saturated porous media embedded in microchannels,” *International Communications in Heat and Mass Transfer,* vol. 57, pp. 309-318, 2014.

[20] T. W. Ting, Y. M. Hung and N. Guo, “Viscous dissipative nanofluid convection in asymmetrically heated porous microchannels with solid-phase heat generation,” *nternational Communications in Heat and Mass Transfer ,* vol. 68, pp. 236-247, 2015.

[21] A. Servati, . K. Javaherdeh and H. R. Ashorynejad, “Magnetic field effects on force convection flow of a nanofluid in a channel partially filled with porous media using Lattice Boltzmann Method.,” *Advanced Powder Technology ,* vol. 25, no. 2, pp. 566-675, 2014.

[22] M. Siavashi, H. R. T. Bahrami and H. Saffari, “Numerical investigation of flow characteristics, heat transfer and entropy generation of nanofluid flow inside an annular pipe partially or completely filled with porous media using two-phase mixture model.,” *Energy,* vol. 93, pp. 2451-2466, 2015.

[23] N. Bachok, A. Ishak and I. Pop, “Flow and heat transfer over a rotating porous disk in a nanofluid,” *Physica B: Condensed Matter,* vol. 406, no. 9, pp. 1767-1772, 2011.

[24] M. Hatami, M. Sheikholeslami and D. Ganji, “Laminar flow and heat transfer of nanofluid between contracting and rotating disks by least square method,” *Powder Technology,* vol. 253, pp. 769-779, 2014.

[25] Hosseini, E. Mohammadian, M. Shirvani, S. Mirzababaei and F. Shakeri Aski, “Thermal analysis of rotating system with porous plate using nanofluid.,” *Powder Technology,* vol. 254, pp. 563-571, 2014.

[26] I. Dincer and M. Rosen, " Exergy: energy, environment and sustainable development," *Newnes,* 2012.

[27] M. Torabi, G. Peterson and N. Karimi, "A thermodynamic analysis of forced convection through porous media using pore scale modeling," *International Journal of Heat and mass Transfer,* vol. 99, pp. 303-316, 2016.

[28] M. Torabi, K. Zhang, N. Karimi and G. Peterson, "Entropy generation in thermal systems with solid structures-a concise review," *International Journal of Heat and Mass Transfer,* vol. 97, pp. 917-931, 2016.

[29] M. Torabi, K. Zhang and S. Mahmud, "Temperature and Entropy Generation Analyses Between and Inside Rotating Cylinders Using Copper–Water Nanofluid," *Journal of Heat Transfer,* vol. 137, no. 5, p. 051701, 2015.

[30] A. Hasanpour, M. Farhadi, K. Sedighi and H. Ashorynejad, "Numerical study of Prandtl effect on MHD flow at a lid-driven porous cavity," *International Journal for Numerical Methods in Fluids,* vol. 70, no. 7, pp. 886-898, 2012.

[31] O. Mahian, A. Kianifar, C. Kleinstreuer, A.-N. Moh'd A, I. Pop, A. Z. Sahin and S. Wongwises, "A review of entropy generation in nanofluid flow," *International Journal of Heat and Mass Transfer,* vol. 65, pp. 514-532, 2013.

[32] M. M. Rashidi, S. Abelman and N. F. Mehr, "Entropy generation in steady MHD flow due to a rotating porous disk in a nanofluid.," *International Journal of Heat and Mass Transfer,* vol. 62, pp. 515-525, 2013.

[33] T. W. Ting, Y. M. Hung and N. Guo, "Entropy generation of viscous dissipative nanofluid convection in asymmetrically heated porous microchannels with solid-phase heat generation.," *Energy Conversion and Management ,* vol. 105, pp. 731-745, 2015.

[34] T. W. Ting, Y. M. Hung and N. Guo, "Entropy generation of viscous dissipative nanofluid flow in thermal non-equilibrium porous media embedded in microchannels," *International Journal of Heat and Mass Transfer,* vol. 81, pp. 862-877, 2015.

[35] E. Ucar, M. Mobedi and I. Pop, "Effect of an inserted porous layer located at a wall of a parallel plate channel on forced convection heat transfer," *Transport in porous media,* vol. 98, no. 1, pp. 35-57, 2013.

[36] M. Nimvari, M. Maerefat and M. El-Hossaini, "Numerical simulation of turbulent flow and heat transfer in a channel partially filled with a porous media," *International Journal of Thermal Sciences,* vol. 60, pp. 131-141, 2012.

[37] N. Karimi, D. Agbo, A. T. Khan and P. L. Younger, "On the effects of exothermicity and endothermicity upon the temperature fields in a partially-filled porous channel," *International Journal of Thermal Sciences,* vol. 96, pp. 128-148, 2015.

[38] S. Mahjoob and K. Vafai, “Analytical characterization and production of an isothermal surface for biological and electronic applications,” 2009.

[39] B. Alazmi and K. Vafai, “Analysis of variants within the porous media transport models,” *Journal of Heat Transfer,* vol. 122, no. 2, pp. 303-326, 2000.

[40] Y. Mahmoudi, N. Karimi and K. Mazaheri, “Analytical investigation of heat transfer enhancement in a channel partially filled with a porous material under local thermal non-equilibrium condition: effects of different thermal boundary conditions at the porous-fluid interface,” *International Journal of Heat and Mass Transfer,* vol. 70, pp. 875-891, 2014.

[41] M. Kavainy, Principles of heat transfer in porous media, Springer Science & Business Media, 2012.

[42] N. Karimi, Y. Mahmoudi and K. Mazaheri, “Temperature fields in a channel partially-filled with a porous material under local thermal non-equilibrium condition-an exact solution,” *Proceedings of the Institution of Mechanical Engineering, Part C, Journal of Mechanical Engineering Science,* vol. 228, no. 15, pp. 2778-2789, 2014.

[43] M. Torabi, N. Karimi and K. Zang, “Heat transfer and second law analyses of forced convection in a channel partially filled by porous media and featuring internal heat sources,” *Energy,* vol. 93, pp. 106-127, 2015.

[44] M. Torabi, K. Zang, G. Yang, Y. Wang and P. Wu, “Heat transfer and entropy generation analyses in a channel partially filled with porous media using local thermal non-equilibrium model,” *Energy,* vol. 82, pp. 922-938, 2015.

[45] K. Yang and K. Vafai, “Analysis of temperature gradient bifurcation in porous media–an exact solution,” *International Journal of Heat and Mass Transfer,* vol. 53, no. 19, pp. 4316-4325, 2010.

[46] O. Mahian, A. Kianifar, Z. Heris and S. Wongwises, “ Natural convection of silica nanofluids in square and triangular enclosures: Theoretical and experimental study,” *International Journal of Heat and Mass Transfer,* vol. 99, p. 792–804, 2016.

[47] S. Salvati, A. Kianifar, H. Niazmand, O. Mahian and S. Wongwises, “ Experimental investigation on the thermal efficiency and performance characteristics of a flat plate solar collector using SiO2/EG–water nanofluids.,” *International Communications in Heat and Mass Transfer,* p. 71–75, 2015.

[48] Z. Xu, Z. Qu, C. Zhao and W. Tao, “Pool boiling heat transfer on open-celled metallic foam sintered surface under saturation condition.,” *International Journal of Heat and Mass Transfer,* vol. 54, no. 17-18, p. 3856–3867, 2011.

[49] J. Buongiorno, “Convective Transport in Nanofluids,” *Journal of Heat Transfer,* vol. 128, no. 3, p. 240, 2006.

[50] M. Sheikholeslami, D. Domiri Ganji, M. Younus Javed and R. Ellahi, “Effect of thermal radiation on magnetohydrodynamics nanofluid flow and heat transfer by means of two phase model,” *Journal of Magnetism and Magnetic Materials,* vol. 374, pp. 36-43, 2015.

[51] M. Sheikholeslami, M. Hatami and G. Domairry, “Numerical simulation of two phase unsteady nanofluid flow and heat transfer between parallel plates in presence of time dependent magnetic field.,” *Journal of the Taiwan Institute of Chemical Engineers,* vol. 46, p. 43–50, 2015.

[52] K. Yang and K. Vafai, “Analysis of heat flux bifurcation inside porous media incorporating inertial and dispersion effects - an exact solution,” *International Journal of Heat and Mass Transfer,* vol. 70, pp. 875-891, 2014.

[53] P. Vadasz, Emerging Topics in Heat and Mass Transfer in Porous Media, Berlin: Springer, 2008.

[54] M. Sheikholeslami, M. Bandpy, M. Ellahi, R. Hassan and S. Soleimani, “Effects of MHD on Cu-Water Nanofluid Flow and Heat Transfer by Means of CVFEM,” *Journal of Magnetism and Magnetic Materials,* vol. 349, pp. 188-200, 2014.

[55] M. Sheikholeslami, D. Ganji and H. Ashorynejad, “Investigation of Squeezing Unsteady Nanofluid Flow using ADM,” *Powder Technology,* vol. 239, pp. 259-265, 2013.

[56] M. Bozorg, M. Fasano, A. Cardellini, A. Chiavazzo and P. Asinari, “A review on the heat and mass transfer phenomena in nanofluid coolants with special focus on automotive applications,” *Renewable and Sustainable Energy Reviews,* vol. 60, pp. 1615-1633, 2015.

[57] T. Zhang and D. Che, “Double MRT thermal lattice Boltzmann simulation for MHD natural convection of nanofluids in an inclined cavity with four square heat sources,” *International Journal of Heat and Mass Transfer,* vol. 94, p. 87–100, 2016.

[58] J. Khan, M. Mustafa and A. Mushtaq, “On three-dimensional flow of nanofluids past a convectively heated deformable surface: A numerical study,” *International Journal of Heat and Mass Transfer,* vol. 94, pp. 49-55, 2016.

[59] A. Purusothaman, N. Nithyadevi, H. Oztop, V. Divya and K. Al-Salem, “Three dimensional numerical analysis of natural convection cooling with an array of discrete heaters embedded in nanofluid filled enclosure,” *Advanced Powder Technology,* vol. 27, no. 1, p. 268–280, 2016.

[60] W. Roshenow and J. Hartnett, Handbook of Heat Transfer, Third ed., New York: McGraw- Hill, 1998.

[61] O. Cekmer, M. Mobedi, B. Ozerdem and I. Pop, “Fully developed forced convection in a parallel plate channel with a centered porous layer,” *Transport in porous media,* vol. 93, no. 1, pp. 179-201, 2012.

1
2

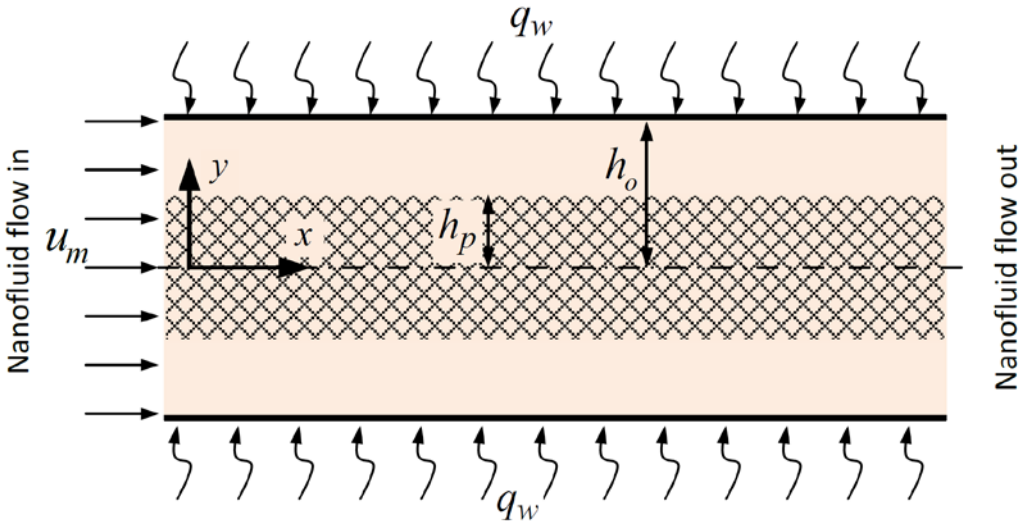

Fig. 1. Schematic configuration of the channel partially-filled with a porous material.

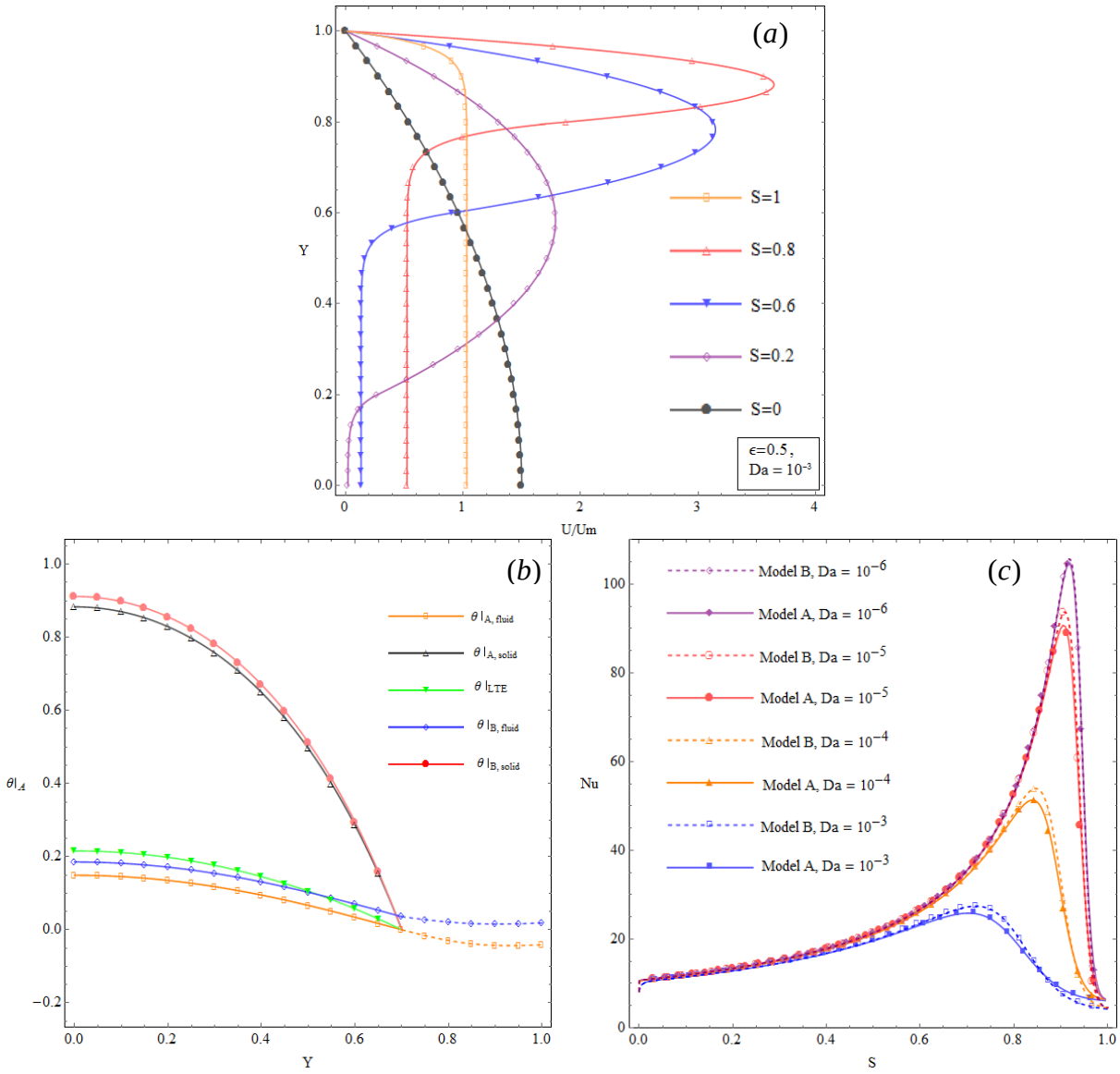

Fig. 2. Validation of the current results at ϕ=0% against the previously published data, (a) velocity compared with Ref. [37], (b) temperature compared with Ref. [37] and (c) Nusselt number compared with Ref. [40].

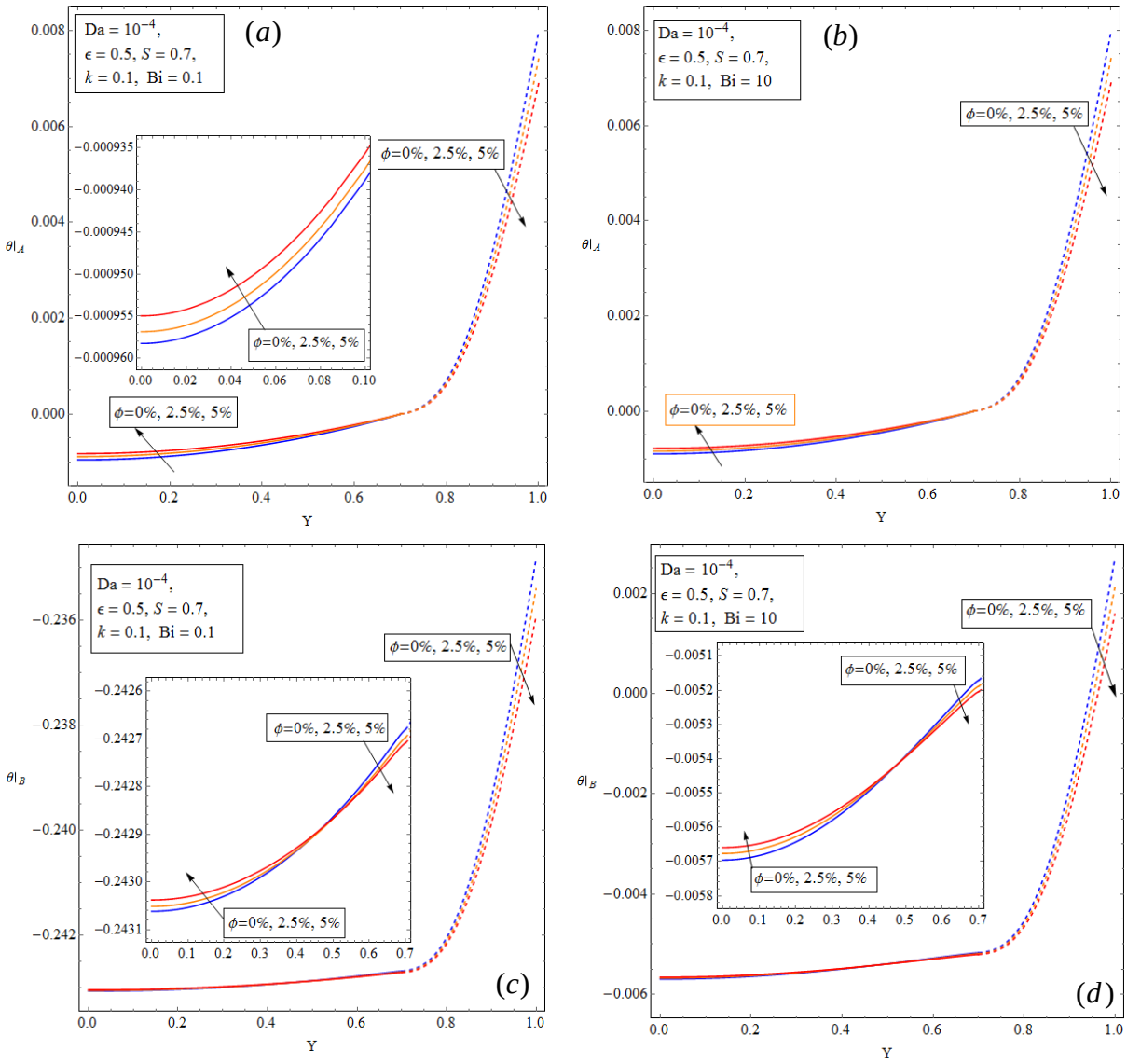

Fig. 3. Dimensionless nanofluid phase temperature distribution under Models A and B and different values of Bi and nanoparticles concentration, k=0.1.

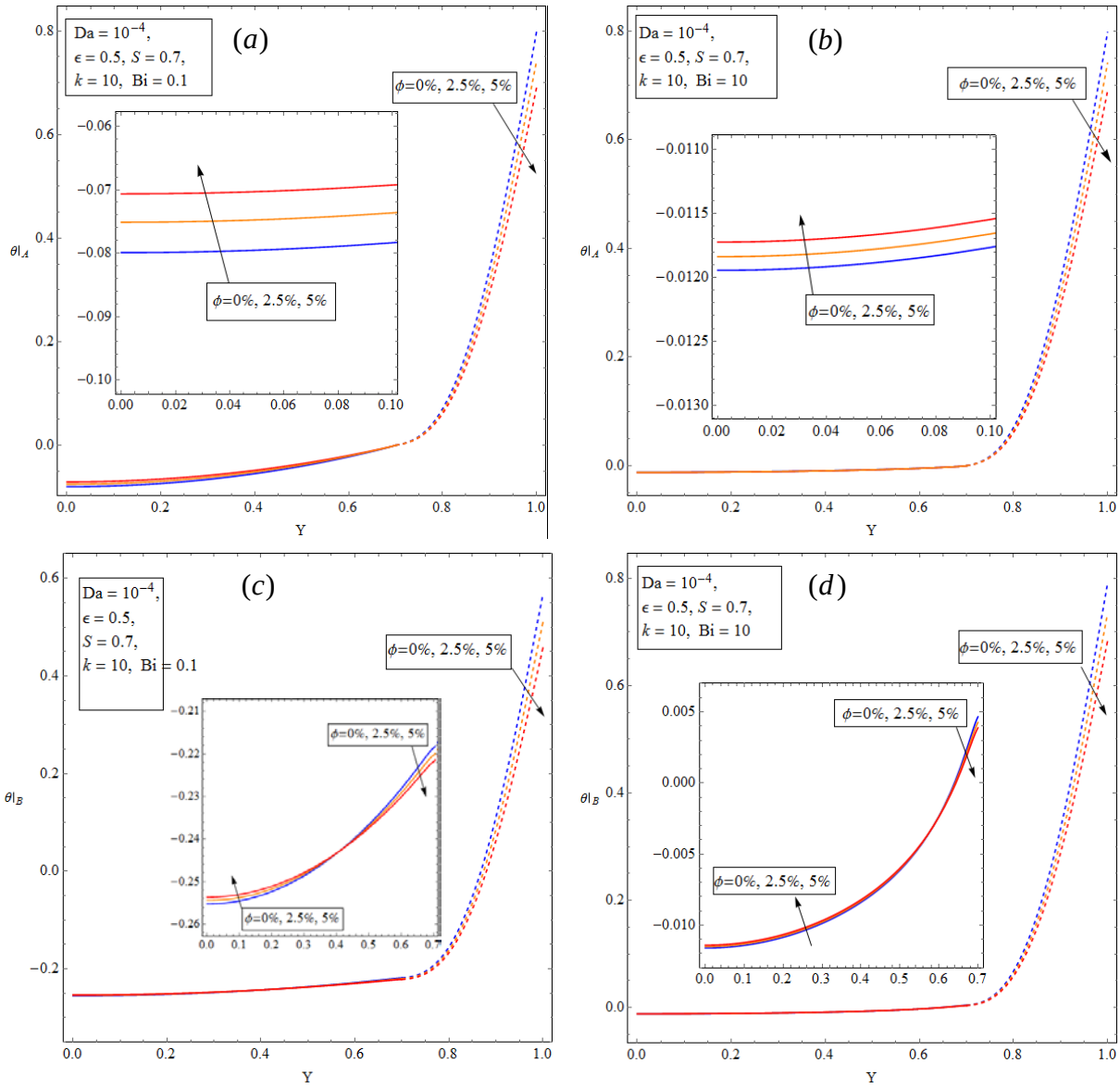

Fig. 4. Dimensionless nanofluid phase temperature distribution under Models A and B and different values for Bi and nanoparticles concentration, k=10.

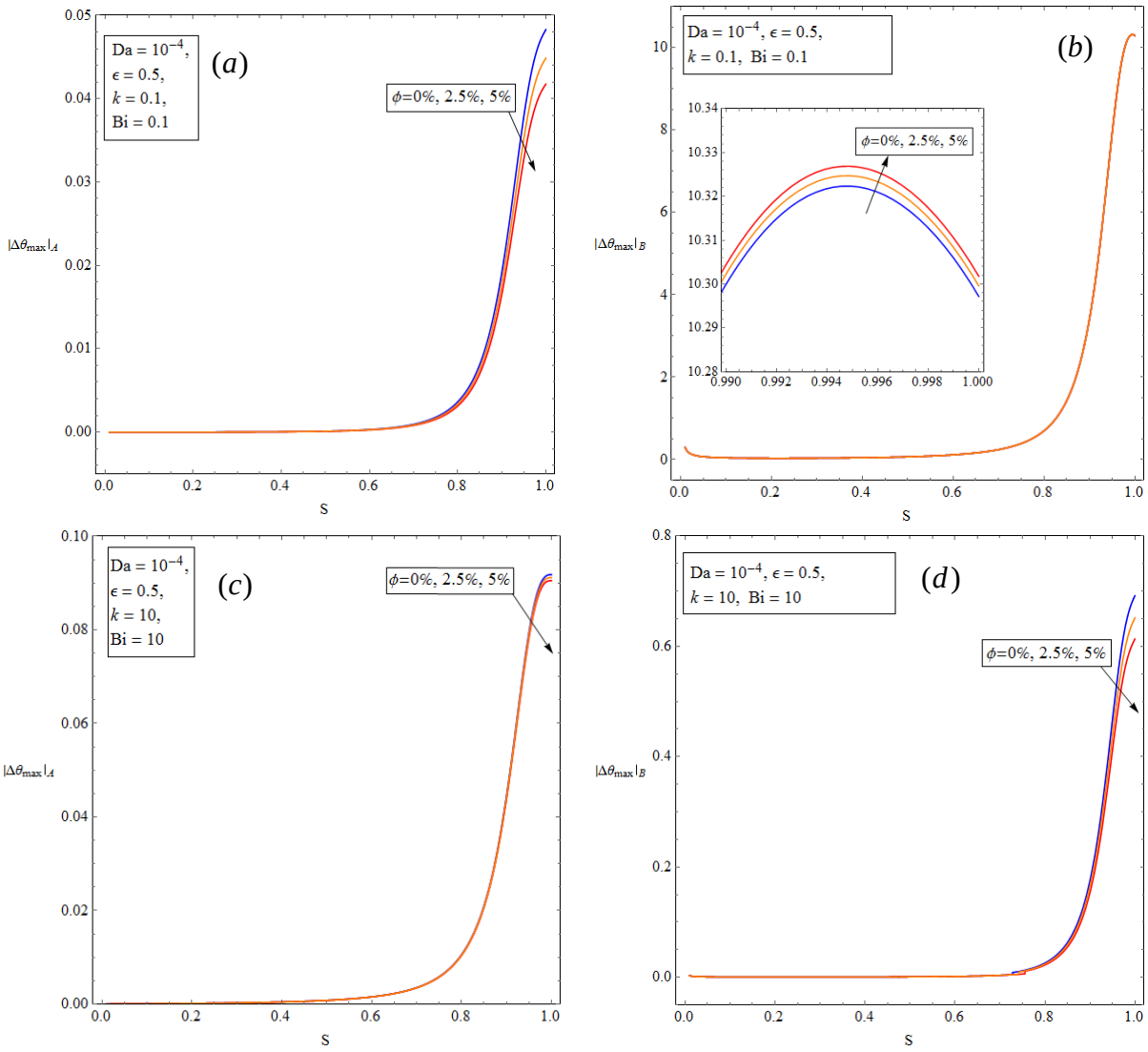

Fig. 5. Maximum temperature difference between the solid and nanofluid phases within the porous insert, Bi=0.1 and k=0.1 for Model A (*a*) and model B (*b*), Bi=10 and k=10 for model A (c) and model B (d).

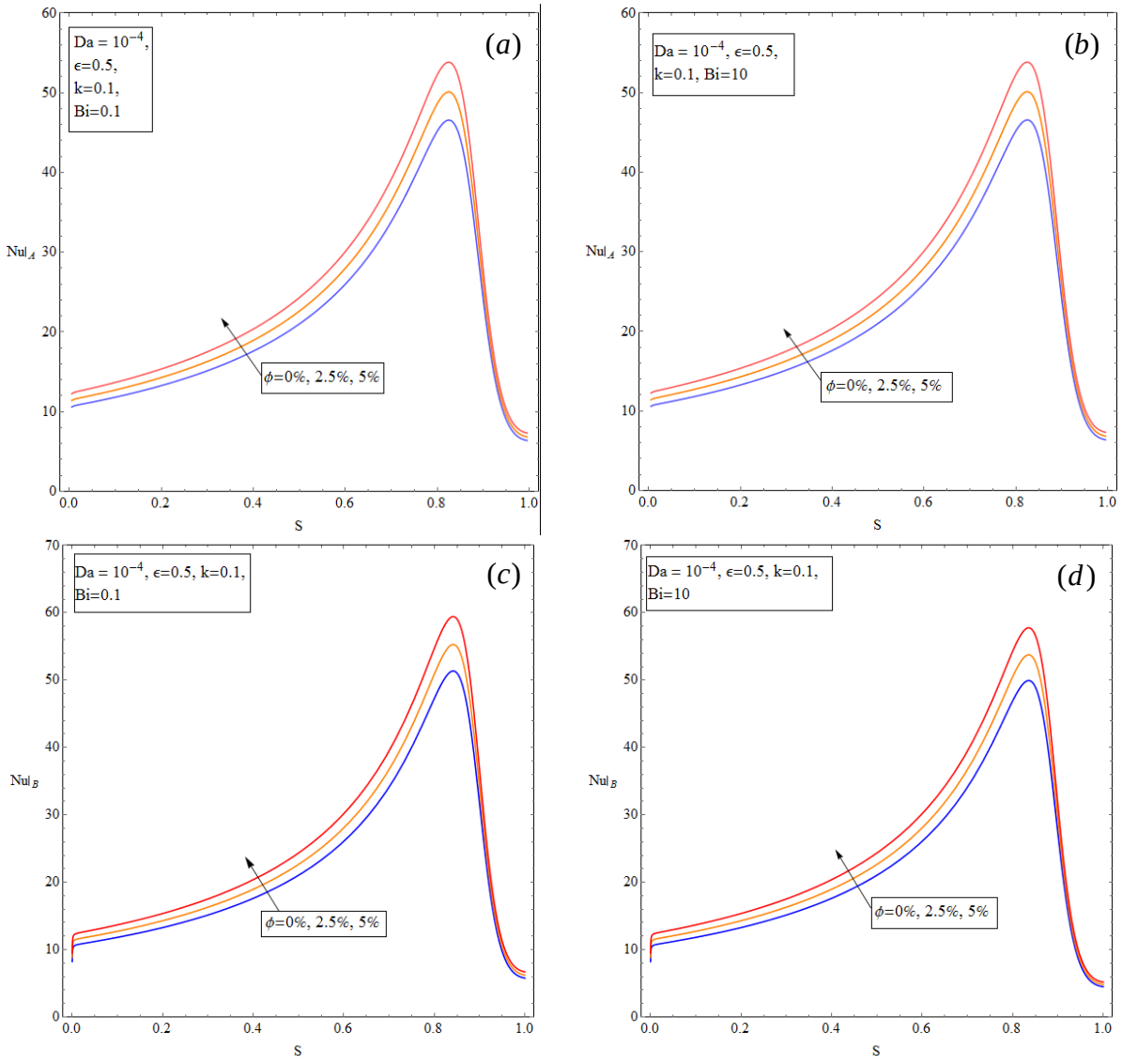

Fig. 6. Nusselt number Models A and B versus the porous thickness for different values of nanoparticles concentration and Bi, k=0.1.

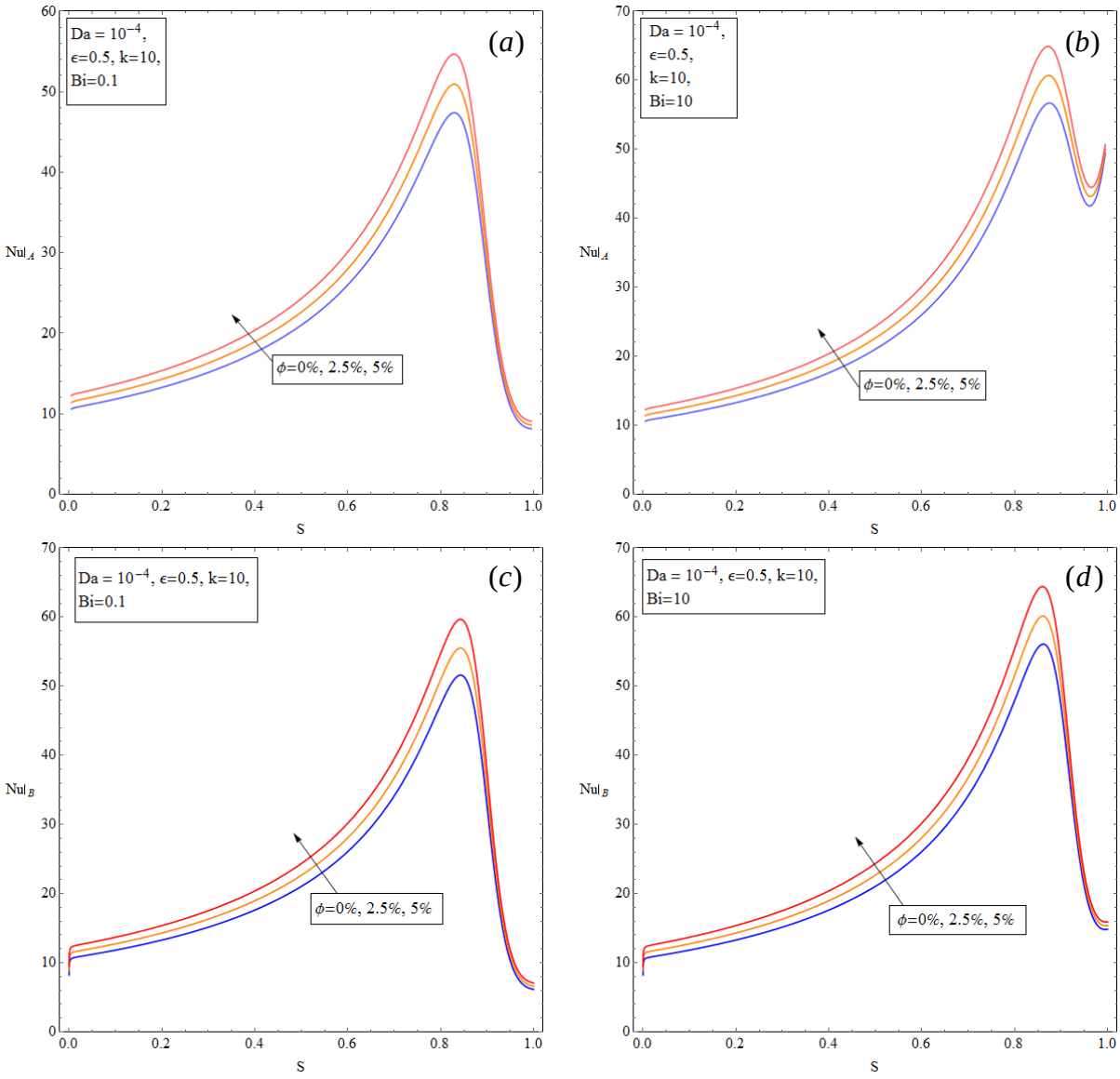

Fig. 7. Nusselt number models A and B versus the porous thickness for different values for nanoparticles concentration and Bi, k=10.

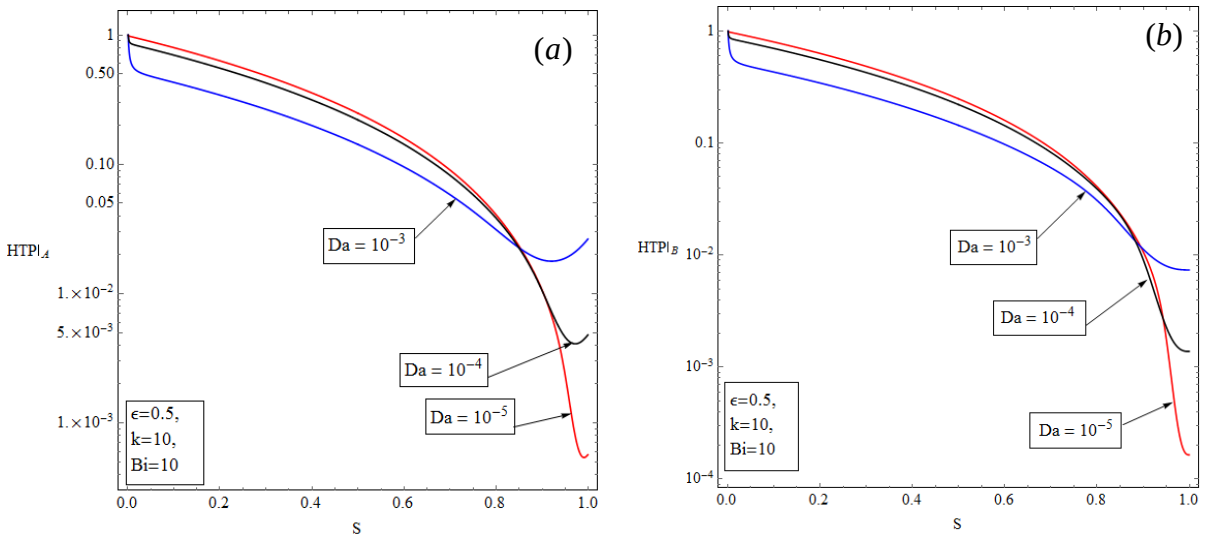

Fig. 8. Heat transfer performance (HTP) under Model A (*a*) and model B (*b*).

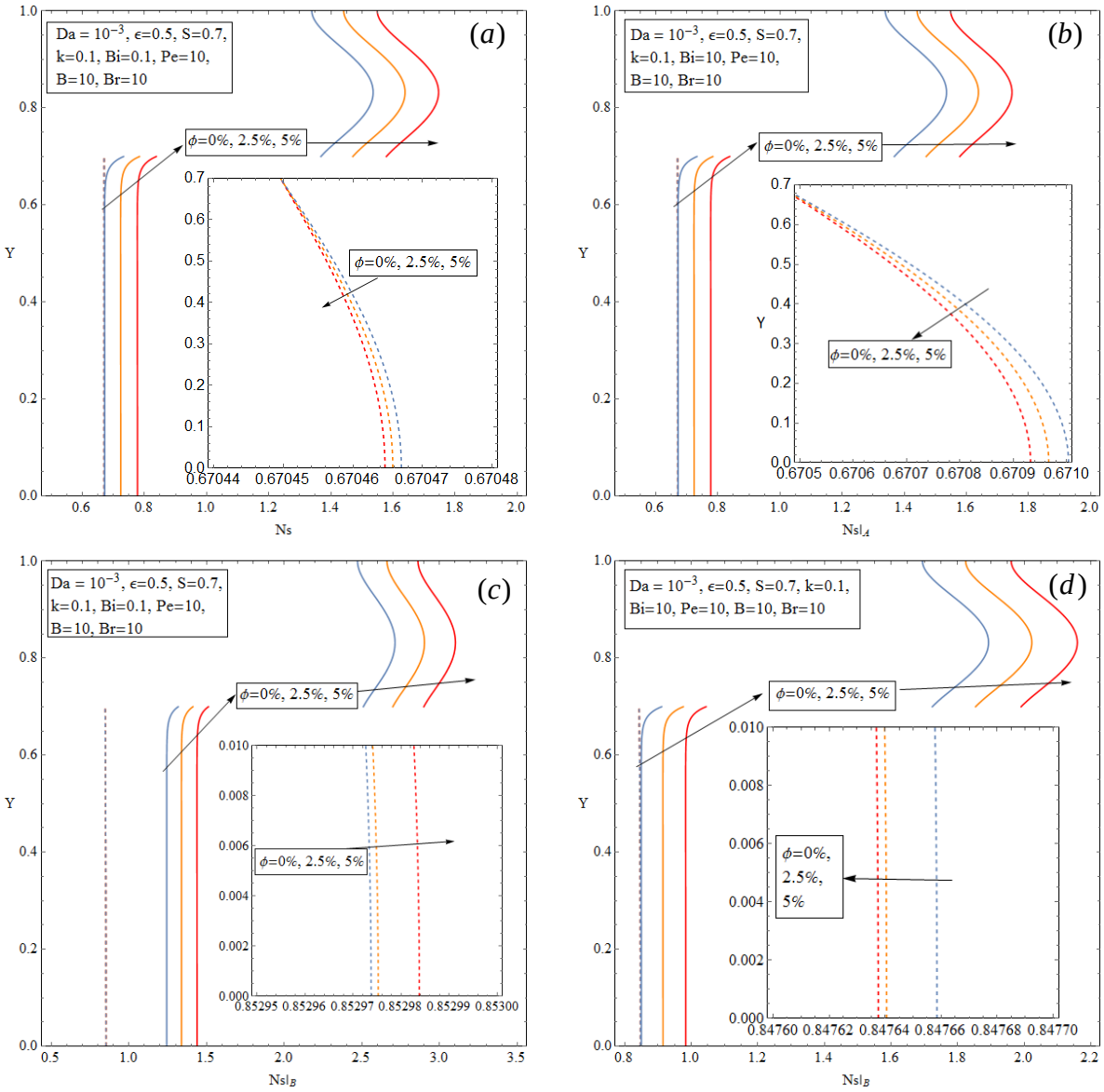

Fig. 9. Dimensionless local entropy generation rate for Models A and B and different values of Bi and nanoparticles concentration, k=0.1 (dash line for solid phase and solid line for fluid phase).

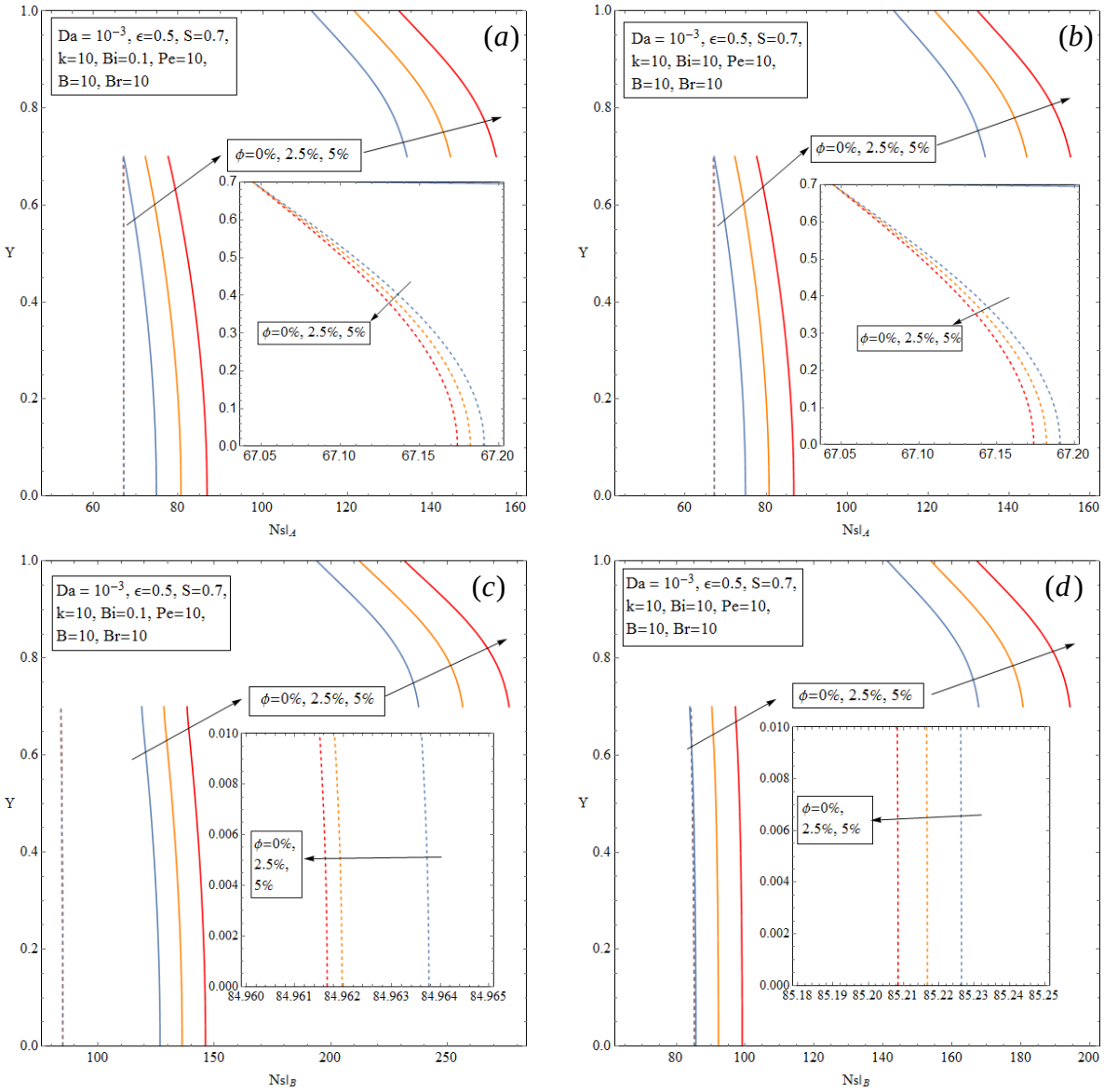

Fig. 10. Dimensionless local entropy generation rate for Models A and B and different values of Bi and nanoparticles concentration, *k*=10 (dash line for solid phase and solid line for fluid phase).

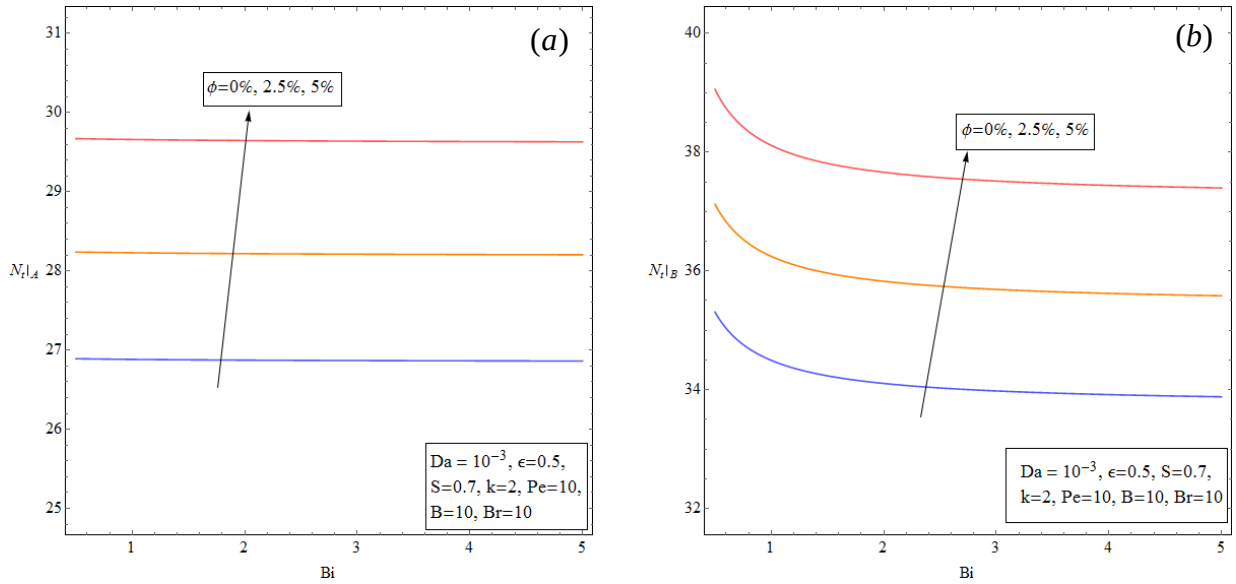

Fig. 11. Total entropy generation rate for Models A and B versus Bi and different values of nanoparticles concentration.

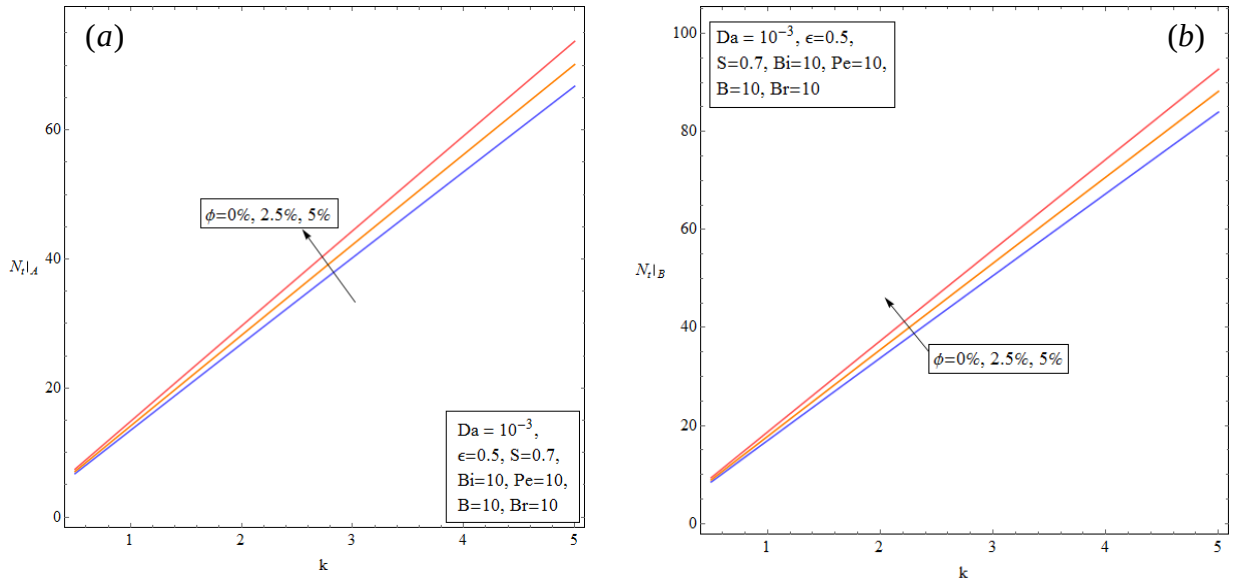

Fig. 12. Total entropy generation rate for Models A and B versus thermal conductivity ratio and different values for nanoparticles concentration.

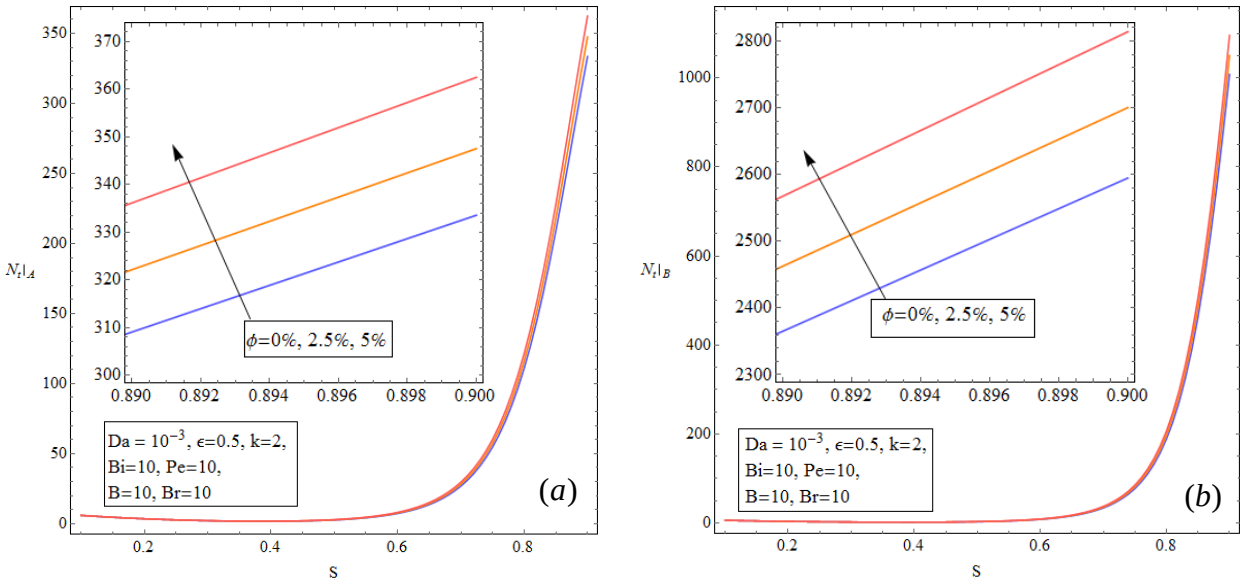

Fig. 13. Total entropy generation rate for Models A and B versus the porous insert thickness and different values of nanoparticles concentration.

Table 1. Representative values for R_μ and R_k based on different concentration rates**.**

ϕ	R_μ	R_k
0.0 (0%)	1.0	1.0
0.025 (2.5%)	1.0653	1.07656
0.05 (5%)	1.1368	1.15714